SIGNATURES OF THE EL NINO-SOUTHERN OSCILLATION ON RAINFALL AND CAVE DRIPWATER OXYGEN ISOTOPES IN N. BORNEO

A Thesis
Presented to
The Academic Faculty

by

Shelby Ann Ellis

In Partial Fulfillment
of the requirements for the Degree
of Masters of Science in the
School of Earth and Atmospheric Sciences

Georgia Institute of Technology
December 2019

SIGNATURES OF THE EL NINO-SOUTHERN OSCILLATION ON RAINFALL AND CAVE DRIPWATER OXYGEN ISOTOPES IN N. BORNEO

Approved by:

Dr. Kim M. Cobb, Advisor
School of Earth and Atmospheric Sciences
Georgia Institute of Technology

Dr. Jean Lynch-Stieglitz
School of Earth and Atmospheric Sciences
Georgia Institute of Technology

Dr. Chris T. Reinhard
School of Earth and Atmospheric Sciences
Georgia Institute of Technology

Date Approved: December 5th, 2019

ACKNOWLEDGEMENTS

To my parents, Tim and Lori Ellis. There are no words that can express the gratitude I feel for your support during all of my years of schooling. You always believed in me, even when I didn't believe in myself. Thank you and I love you.

To all of my close friends (#AerosolForcingsMatter, #PaleoFantasies), acquaintances, faculty, and staff at Georgia Tech: thank you for some of the best (and most stressful) memories of my life! #TeamPaleo: Ya'll kept me afloat in this sea of knowledge that is GT. Made me laugh, smile, held me when I cried, bought me shots of tequila when I didn't think I could fit any more studying into my brain…You all showed me what it is to work in a supporting and loving work environment, where you only strive to lift others up and help them when they are down. I never would have made it this far without your constant guidance, love, and kind words. And awkwardly long hugs from yours truly. This song is for you, from the lead singer of Phish, Trey Anastasio ;)

So this is it
It's over
I don't wanna look
Cause I don't want it to end

Cause I've traveled all over this big ol' world
And it's so hard to find a real friend

People come and people go
In and out of your life
And it don't take long to realize
The real thing don't come everyday

When I was up I had so many friends
When I went down they were gone so fast
And you were always the one who stayed

And why do we have to wait until it's gone
To know what love is

TABLE OF CONTENTS

LIST OF FIGURES

LIST OF SYMBOLS AND ABBREVIATIONS

$\delta^{18}O$	Oxygen isotopic composition
$\delta^{18}O_D$	Mulu dripwater oxygen isotope composition
$\delta^{18}O_R$	Mulu rainfall oxygen isotope composition
$\delta^{18}O_{stal}$	Stalagmite oxygen isotopic composition
δD	Hydrogen isotopic composition
‰	Per mil or per thousand
1σ	One standard deviation
40:60	40% contribution from Reservoir A and 60% contribution Reservoir B
80:20	80% contribution from Reservoir A and 20% contribution Reservoir B
ARM	Autogenic Recharge Model
BMM	Bivariate Mixing Model
dpm	Drips per minute
ENSO	El Niño-Southern Oscillation
ERSSTv5	Extended Reconstructed Sea Surface Temperatures version 5

GCM	Global circulation model
GHGs	Greenhouse gases
GMWL	Global meteoric water line
ITCZ	Intertropical convergence zone
IAEA	International Atomic Energy Agency
JFM	January-February-March
L2	“Lang’s Cave” drip site
LMWL	Local meteoric water line
Niño 3	Boxed region of 150ºW-90ºW and 5ºN-5ºS
Niño 3.4	Boxed region of 170ºW-120ºW and 5ºN-5ºS
Niño 4	Boxed region of 160ºE-150ºW and 5ºN-5ºS
NIST	National Institute of Standards and Technology
OISST	Optimum interpolation sea surface temperature
OLR	Outgoing longwave radiation
OND	October-November-December
SOI	Southern Oscillation Index

SST	Sea surface temperature
SSTa	Sea surface temperature anomaly
U/Th	Uranium/Thorium series
V-PDB	Vienna-Pee Dee Belemnite
V-SMOW	Vienna-Standard Mean Ocean Water
V-SLAP	Vienna-Standard Light Antarctica Water
WF	“Wind Fast” drip site
WPWP	West Pacific Warm Pool
WS	“Wind Slow” drip site

SUMMARY

Oxygen isotope ($\delta^{18}O$) records of speleothem carbonates are a critical terrestrial paleoclimate archive, providing insight into past hydroclimate variations and past changes in atmospheric circulation. Specifically, time series of rainfall and cave dripwater oxygen isotopes ($\delta^{18}O$) provide site-specific assessments of climate or non-climate related signals recorded in stalagmite $\delta^{18}O$ used for such reconstructions. However, modern paired multi-year $\delta^{18}O$ time series of rainwater and dripwater are limited in the tropical latitudes, an area known to contain regionally-specific atmospheric complexities acting on rainfall $\delta^{18}O$. Furthermore, karst drainage pathways vary significantly within the same cave system, altering the original climate-driven $\delta^{18}O$ rainfall signal. In this thesis, I present an extended multi-year study of rainfall and cave dripwater $\delta^{18}O$ time series from Gunung Mulu National Park in Northern Borneo to quantify the cloud-to-cave transformation process spatially and temporally across the Mulu karst, building on work previously presented by Moerman et al., 2013 and Moerman et al., 2014.

Chapter 1 will broadly cover topics related to how stable water isotopes in rainfall, cave dripwaters, and stalagmites can detect ENSO-driven shifts in the hydrological cycle, building off almost a decade's worth of modern (Cobb et al., 2007; Moerman et al., 2013; 2014; Partin et al., 2013a) and paleoclimate (Carolin et al., 2013; 2016; Chen et al., 2016; Meckler et al., 2012; Partin et al., 2007; 2013a) observations from a well-established research site in Northern Borneo, Sarawak, Malaysia.

Chapter 2 quantifies the rainfall-to-cave dripwater transformation of isotopic climate-signals in the Mulu karst from continuous observations over the last ~12 years.

These time series are the longest-running daily rainfall $\delta^{18}O$ time series (2006 – 2018) and longest tropical biweekly dripwater $\delta^{18}O$ time series (2007 – 2018) globally. Vadose zone mixing translates ENSO-related variations in rainfall $\delta^{18}O$ to three monitored cave dripwater $\delta^{18}O$ sites. Using two simple modeling techniques, we generated an ensemble of different modeled dripwater time series directly corresponding to local rainfall $\delta^{18}O$, estimating Mulu water takes ~3 to 18 months to transit through the karst. This transit time provides context for what resolution of climate signals can be potentially recorded in local stalagmites employed for hydroclimate reconstructions. Overall, this thesis supports previous interpretations of using the amount effect framework for Mulu stalagmite $\delta^{18}O$ records through the multi-year, paired local rainfall and dripwater $\delta^{18}O$ time series. This research clearly demonstrates paired rainfall and cave $\delta^{18}O$ observations can support more minute interpretations of highly-resolved paleo-ENSO stalagmite records.

CHAPTER 1. INTRODUCTION

Developing nations in the tropics reliant on rainfall for freshwater and agricultural security are predicted to accommodate more than half of the world's population by 2050 (State of the Tropics Report, 2017). However, rainfall is predicted to change significantly in response to anthropogenic greenhouse gas (GHG) forcings (Chadwick et al., 2013), threatening freshwater security in these populous nations. Yet the magnitude and location of future rainfall shifts remain uncertain (Chadwick et al., 2013). Specifically, model uncertainties surrounding future variability associated with the coupled ocean-atmosphere phenomenon El Niño-Southern Oscillation (ENSO) remain relatively large (Bellenger et al., 2014; Lu et al., 2018), limiting the skill of tropical rainfall projections (Christensen et al., 2013; Collins et al., 2010). Some studies predict a near doubling in the frequency of El Niño events in response to increased GHGs (Cai et al., 2014; Wang et al., 2017), suggesting large-scale atmospheric reorganizations in the tropics and subtropics interannually. This has already been observed through multiple very strong El Niño events (1982/1983, 1997/1998, and 2015/2016), critically altering global weather patterns and ecosystems via droughts, floods, and extreme weather events (Glynn and Weerdt, 1991; Nakagawa et al., 2000). Because such events can profoundly alter freshwater security, predicting ENSO's behavior in a warming world has become one of the most pressing climate challenges.

Climate models rely heavily on observational datasets to project future regional climate trends. However, rainfall records in many tropical regions are too short and sparse to fully characterize natural climate variability. The paucity of instrumental records has scientists turning towards paleoclimate archives such as stalagmites, which have the ability to be

precisely dated and to geochemically record climate signals in their calcite matrix. The ability to record climate signals in stalagmite calcite relies on the fact that cave dripwater $\delta^{18}O$ composition reflects rainfall $\delta^{18}O$ variability which is linked to large-scale hydrological variability. Thus, in order to understand how climate is recorded in stalagmites from a given site, scientists must compare the rainfall $\delta^{18}O$ to large-scale climate, and then compare dripwater $\delta^{18}O$ variability to rainfall $\delta^{18}O$ variability to constrain the relative influence of climate- versus karst-driven processes on dripwter $\delta^{18}O$. The work addressed here investigates the isotopic response of rainfall and cave dripwaters to individual ENSO events in N. Borneo, a region that boasts many previous stalagmite-based hydrological reconstructions of the West Pacific Warm Pool (WPWP) over the last 500,000 years (Carolin et al., 2013, 2016; Chen et al., 2016; Meckler et al., 2012; Partin et al., 2007, 2013a).

1.1 Stable water isotopes as tracers of Earth's Hydrosphere

1.1.1 Stable water isotopes

Stalagmite $\delta^{18}O$ records track small variations in the ratio of two stable oxygen isotopes: ^{16}O and ^{18}O. Stable isotopes are atoms of the same element that contain a different number of neutrons, driving differences in their overall masses, described as a mass number. The combination of two stable Hydrogen and one Oxygen isotope generate 'water isotopologues (i.e. $^{1}H_2{}^{16}O$, $^{1}H^{2}D^{18}O$, etc.), where water molecules can exist as nine isotopic combinations, with two stable isotopes of hydrogen (^{1}H and ^{2}D) and three of oxygen (^{16}O, ^{17}O, and ^{18}O) (Faure and Mensing, 2005). With regards to oxygen's natural abundances on Earth, stable isotope ^{16}O dominates naturally as the most abundant

(99.76%), while ^{17}O and ^{18}O are significantly less (0.04 and 0.20%, respectively) (Kendall and McDonnell, 1998).

Subtle physio-chemical property differences arise between same-element isotopes because of their mass differences, generating discrepancies in the chemical bond strength found between heavy and light molecules. During reactions or phase changes, these molecules undergo mass-dependent isotopic fractionation. This fractionation preferentially partitions isotopes between two substances (e.g. water versus calcite) or phases (e.g. liquid/vapor) based on mass-dependent properties such as chemical bond strength. As well, because molecules vibrate at a fundamental frequency dependent on their mass, it is implied heavier isotopes are more stable and react less easily than light isotopes and require a higher dissociation energy to break bonds between molecules (Kendall and McDonnell, 1998). Thus, heavier isotopes during reactions or phase changes are more likely to be incorporated into the more condensed and lower energy substances (e.g. liquid over vapor; calcite over dripwater) (Clark and Fritz, 1997). A clear example of such a phase change is when water vapor cools and condenses from a cloud. This leaves the vapor pool relatively depleted in the heavy isotope (^{18}O) as it was preferentially incorporated into the lower energy phase (e.g. liquid/rain).

Condensation from an air parcel is typically considered an equilibrium fractionation process and is the dominant driver of the isotopic composition of measured rainfall (Clark and Fritz, 1997, Mook, 2001). Equilibrium fractionation is a temperature dependent process where greater fractionation occurs at lower or decreasing temperatures (Mook, 2001). The assumption of equilibrium fractionation during the phase transition between

vapor and liquid are assumed to occur in a closed environment and are fully reversible, where both forward and backward reaction rates are uniform:

$$^{1}H_2{}^{16}O\ (l) + {}^{1}H_2{}^{18}O\ (g) \leftrightarrow {}^{1}H_2{}^{18}O\ (l) + {}^{1}H_2{}^{16}O\ (g)$$

The isotope fractionation related to the equilibrium exchange reaction can be defined by the fractionation factor α:

$$\alpha_{A-B} = \frac{R_A}{R_B} \tag{1}$$

where R represents the ratio of heavy (A) to light (B) isotopes of a given phase (Hoefs, 2004). The ratio of heavy to light isotopes in oxygen analyzed on mass spectrometers are most commonly reported in δ notation relative to the international standard $^{18}O/^{16}O$ ratio in units of per mil (‰):

$$\delta^{18}O = \left(\frac{\frac{^{18}O}{^{16}O_{\text{sample}}} - \frac{^{18}O}{^{16}O_{\text{standard}}}}{\frac{^{18}O}{^{16}O_{\text{standard}}}} \right) \times 1000 \tag{2}$$

Reported international standards are V-SMOW (Vienna-Standard Mean Ocean Water) for liquid samples and V-PDB (Vienna-Pee Dee Belemnite) for carbonate-based samples (i.e. stalagmites) with a $\delta^{18}O$ value of 0‰. If a sample has a reported value that is negative (positive), this indicates a lower (higher) $^{18}O/^{16}O$ ratio than the standard. Commonly, a more negative $\delta^{18}O$ value is said to be isotopically 'depleted' or 'lighter' while more positive $\delta^{18}O$ values are 'more enriched' or 'heavier'.

Under equilibrium conditions, $\delta^{18}O$ and $\delta^{2}D$ values in meteoric water samples vary in tandem and in a linear fashion (Craig, 1961; Dansgaard, 1964; Rozanski et al., 1993) by the equation:

$$\delta^{2}D = 8(\delta^{18}O) + 10 \tag{3}$$

This linear equation characterizes the relationship between hydrogen and oxygen in global fresh surface waters, called the Global Meteoric Water Line (GMWL). The slope of ~8 represents that under equilibrium conditions, hydrogen isotopic fractionation is almost 8x more efficient than oxygen fractionation due to hydrogen's smaller binding energy and differences in vapor pressure (Hoefs, 2004; Majoube, 1971). Modern precipitation and groundwater investigations, when possible, should characterize the local relationship between $\delta^{18}O$ and δD since the local meteoric water line (LMWL) can differ substantially from the GMWL.

Most generally, the combination of various isotope effects generates spatially consistent, coherent variations in rainfall $\delta^{18}O$ related to latitude, altitude, and moisture source (Bowen and Wilkinson, 2002; Dansgaard, 1964; Rozanski et al., 1993). These empirically-based 'isotope effects' (e.g. temperature, altitude, continental, source, and amount effect) are most commonly visualized to the first order by the Rayleigh distillation model, showing the progressive cooling and rainout of a singular air mass as it moves along a trajectory path. In this model, the removal of moisture from an air mass is temperature-dependent, with the amount of moisture condensed from the cloud proportional to the drop in temperature (Dansgaard, 1964). However, when considering a single site, a more in depth explanation is needed to explain local $\delta^{18}O_R$ variability, given the multitude of influencing climatological and geographic factors such as topography, air mass mixing, moisture source, or residing climate regime. In tropical regions that undergo deep vertical convection such as N. Borneo, the 'amount effect' dominates $\delta^{18}O_R$ variability and will be discussed in short in the following section.

1.1.2 The Amount Effect

The amount effect is an empirically-derived relationship, wherby high (low) rainfall rates on monthly and longer time scales are correlated with depleted (enriched) $\delta^{18}O_R$ (Dansgaard, 1964; Rozanski et al., 1993). However, independent tropical observations (Sanchez-Murillo et al., 2016; Zwart et al., 2018) and isotope-enabled general circulation models (GCMs) (Conroy et al., 2013) highlight other factors controlling tropical $\delta^{18}O_R$ beyond local rainfall amount. This is because multiple competing processes act at an individual site given its unique orographic variations or localized wind patterns (Konecky et al., 2019). Other factors observed to control local tropical $\delta^{18}O_R$ beyond the amount effect include proportions of convective vs. stratiform clouds (Aggarwal et al., 2016; Kurita, 2013), changes in moisture source (Cai and Tian, 2016; Konecky et al., 2019; Okazaki et al., 2016), or amount of upstream rainout and subsequent re-evaporation of falling rain drops (Konecky et al., 2019).

Currently, the 'amount effect' is used to infer hydrological variability from speleothem $\delta^{18}O$ records, where lower (higher) calcite $\delta^{18}O$ values indicate wetter (drier) conditions. However, the individual processes acting on local $\delta^{18}O_R$ at a site, without proper identification, can become further obscured when transformed and recorded within a local paleoclimate proxy and lead to misinterpretations (Evans et al., 2013).

1.1.3. Karst-driven isotopic alteration of groundwaters revealed by cave monitoring

The waters recharging an aquifer are most likely sourced from local rainfall, which in turn feeds cave dripwaters that can precipitate stalagmites under the right geochemical setting. Because the dripping water feeding a stalagmite has a distinct climate-driven isotopic signal that can be transferred to calcite, stalagmites have rocketed to the forefront as a critical terrestrial paleoclimate archive to characterize regional hydroclimate shifts.

However, the complexity of karst environments drives numerous processes that modify the original $\delta^{18}O_R$ signal before emerging as cave dripwaters, complicating stalagmite $\delta^{18}O$ interpretations. Site-specific observations above caves indicate $\delta^{18}O_R$ alteration through evaporative fractionation, isotopically enriching soil waters before infiltrating into karst bedrock (Cuthbert et al., 2014). Further karst complexities altering the $\delta^{18}O_R$ signal reflected in cave dripwater $\delta^{18}O$ (hereinafter $\delta^{18}O_D$) include the amount of reservoir or aquifer stores in the vadose zone due to bedrock/porosity type (Ford and Williams, 2013), whether recharged waters mix with vadose waters of differing isotopic compositions (Fairchild et al., 2006), and preferred recharge flow pathway (Fairchild and Baker, 2012). Preferred flow routing within bedrock prompts discrepancies in the water transit time between surface to cavern, where a combination of such complexities explain why some sites observe large differences in year-to-year $\delta^{18}O_D$ variability from same-cavern sampling (Partin et al., 2013a; Treble et al., 2013; Zhang and Li, 2019). Indeed, modern monitoring of rainfall and cave dripwaters remain crucial to quantify the robustness of the climate-to-calcite isotopic relationship at individual paleoclimate sites, especially those undergoing calibration efforts or the interpretation of highly-resolved stalagmite $\delta^{18}O$ records.

1.2 Forward Proxy System Models

Interpretations of stalagmite records rely on the assumption that the modern isotopic controls over rainfall and cave dripwaters are stationary over much longer time scales and linearity of the karst (i.e. same karst residence time) remains the same through-out the inferred paleodata-climate relationship (Evans et al., 2013). To improve upon these broad assumptions, considerable attention has turned towards investigations of (i) climate processes driving observed modern rainfall $\delta^{18}O$ and (ii) the karsts influence on the

delivery of climate signals in cave dripwater by increased cave monitoring efforts (Wong and Breecker et al., 2015). However, continuous cave monitoring is not always feasible in some remote tropical locations, although new modeling techniques can generalize results from various cave sites aiding interpretations of measured calcite $\delta^{18}O$. Specifically, forward proxy system models (PSMs) predict pseudo-calcite and cave dripwater $\delta^{18}O$ values based on our empirically or theoretically-derived comprehension of how environmental signals, affected from physical, chemical, biological, and geologic processes, are preserved in stalagmite calcite (Evans et al., 2013; Wong and Breecker, 2015). PSMs contain three inherent sub-model components, the sensor, the archive, and the observation, and when applied together can comprehensively model pseudo-calcite $\delta^{18}O$ values. The sensor (i.e. karst system) will have a non-linear and/or multivariate response to a climate forcing, dictating the isotopic composition of cave dripwaters (Evans et al., 2013; Wong and Breecker, 2015). The karsts effect on cave dripwaters dictates the deposition of the stalagmite's calcite, developing unique isotopic, physical, or geochemical characteristics detected through observations. In turn, all three subsystem models respond to climate forcings differently, allowing for error contributions from each subsystem to be more easily identified (Dee et al., 2015).

Two sensor sub-model PSMs were used by Moerman et al., (2014) to make inferences on the best modeled karst residence time (τ) and how τ could impact resolvable climate $\delta^{18}O$ signals in pseudo-stalagmites. The first model generated a suite of modeled cave dripwater $\delta^{18}O$ time series' by increasing weekly-based time lags of daily rainfall $\delta^{18}O$. By comparing these modeled time series to ~6.5 years of cave dripwater observations, inferences to τ were made for individual sites (between 3 – 10 months). The

second sensor sub-model generated two pseudo-stalagmites using the extreme time-ends (3 months and 10 months) of inferred karst residence times. This sensor sub-model indicated that differences in τ had the most significant impact on the variance of high-resolution pseudo-calcite $\delta^{18}O$ signals.

1.3 El Niño-Southern Oscillation

The El Niño-Southern Oscillation (ENSO) is a coupled ocean-atmosphere phenomenon operating in the tropical Pacific that dominants the global mode of interannual climate variability. It has two opposing phases: a warm (El Niño event) and a cold phase (La Niña event). The growth and decay of ENSO events is rooted in positive coupled feedback mechanisms (e.g. the Bjerknes feedback) and in equatorial ocean dynamics. An El Niño event occurs as persistent westerly wind anomalies reduce the wind stress on the ocean, causing the thermocline to deepen, and sea surface temperatures (SSTs) to increase in the central and eastern Pacific. The westerly wind anomalies also trigger equatorial Kelvin waves, deepening the thermocline as they propagate east. Positive SST anomalies in the east enhance the westerly wind anomalies by reducing the zonal gradient of SST and sea level pressure across the Pacific. The weakened eastern trade winds can cause further warming through reduced upwelling of cold water on the equator, giving rise to anomalous ocean currents advecting warm water eastward (down the mean SST gradient). Atmospheric responses to an El Niño event includes an eastward shift of the region of deep convection, producing drying in the WPWP and increased rainfall in the central and eastern Pacific. ENSO events typically last 9 – 12 months, with the timescale dictated by the propagation speed of the equatorial ocean waves (e.g. time it takes upwelling Rossby waves to propagate from the region of wind forcing to the western boundary, where they are

subsequently reflected back eastward as cold equatorial Kelvin waves). Once returning Kelvin waves reach the central and eastern Pacific, cooler waters help re-establish normal ocean and atmosphere conditions. An opposing positive feedback mechanism helps establish the opposing La Niña phase, occurring most often after an El Niño event.

1.4 Gunung Mulu National Park

1.4.1 Climatic Setting

Gunung Mulu National Park (hereinafter called Mulu) in N. Borneo (4°06'N, 114°53'E) is set near the equator generating a lush tropical rainforest setting. This site receives up to 5m of precipitation annually, exhibiting significant intraseasonal and interannual variability (Moerman et al., 2013). An extensive modern rainfall study conducted in 2013 with 5 years of daily resolved precipitation data, demonstrated that Mulu experiences: (1) the majority of its precipitation through discrete convective events in the afternoon, (2) weak seasonality in precipitation with its geographic location within the boundaries of the intertropical convergence zone (ITCZ) seasonal insolation shifts and (3) has the largest departures in precipitation amount and rainfall $\delta^{18}O$ intraseasonally from the Madden-Julian Oscillation (MJO; 30–90 days) and interannually from ENSO (2–7 years). La Niña (El Niño) events deliver anomalously wet (dry) conditions to the region (Cobb et al., 2007, Moerman et al., 2013).

1.4.2 Local Geology

The caverns at Gunung Mulu are part of the Melinau Limestone Formation, a shallow carbonate platform falling within the Upper Eocene-Lower Miocene (Sweeting, 1980; Waltham and Brook, 1980; Gillieson and Clark, 2010). The main formations include carbonate mounds and gorges that are geographically set in the northeast-to-southwest

direction (Figure 1). The deep gorges in the formation were formed by rivers, isolating massive mounds of carbonate, with the highest of the three mounds, Gunung Mulu, found at 2376m above sea level (Cobb et al., 2007; Sweeting, 1980). Sample collection cave chambers are ~120 – 200m above sea level (Carolin et al., 2016), and the high level of cave entrances in the park indicates the rapid transition of the relief via tectonic activity, estimated to occur during the Pleistocene and Holocene (Sweeting, 1980). Much of the drainage of the carbonate platform, which acts to recharge the karst, is through fissured limestone to underground caves or cave rivers (Waltham & Brook, 1980). Other recharge sources include flood waters supplied from the Melinau alluvial plain and allogenic water runoff from the sandstone mountain, Gunung Mulu (Waltham & Brook, 1980; Moerman et al., 2014).

1.4.3 Northern Borneo Stalagmite $\delta^{18}O$ Records

Stalagmites in Northern Borneo at Mulu have reconstructed hydroclimate shifts in the WPWP during the last 500,000 years, showcasing the western tropical Pacific's sensitivity to low and high latitude forcings (Carolin et al., 2013, 2016; Chen et al., 2016; Meckler et al., 2012; Partin et al., 2007). Low-latitude precessional forcing (with a period of ~19 to 23ky) is the dominant source of orbital-scale hydroclimate variability in the west Pacific (Carolin et al., 2016; Meckler et al, 2012; Partin et al., 2007). In addition, high-latitude forcings, such as the abrupt North Atlantic cooling events (Bond et al., 1997), occurs during millennial-scale drying in the west Pacific (Carolin et al., 2013; Partin et al., 2007). Records also indicate a dynamical link between WPWP hydrology and high latitude glacial-interglacial transitions but not with differences in steady-state climate across different interglacial intervals (Meckler et al., 2012). Lastly, Chen et al.

(2016) inferred reduced ENSO variance during the mid-Holocene from an annually resolved stalagmite. Reduced ENSO variance was driven from persistent warm pool convection from a precession-driven maximum in insolation, enhancing easterly winds and suppressing the development of El Niño events (Chen et al., 2016). This suggests the overall mean state of the west Pacific warm pool is a dominant factor in ENSO behavior on millennial and longer timescales (Chen et al., 2016).

CHAPTER 2. CAVE DRIPWATER TIME SERIES CAPTURES THE 2015 – 2016 EL NIÑO EVENT IN N. BORNEO

Time series of cave dripwater oxygen isotopes ($\delta^{18}O$) provide site-specific assessments of the contributions of climate and karst processes to stalagmite $\delta^{18}O$ records employed for hydroclimate reconstructions. We present ~12 year-long time series of biweekly cave dripwater $\delta^{18}O$ variations from three sites along with a daily-resolved local rainfall $\delta^{18}O$ record from Gunung Mulu National Park in Northern Borneo. Mixing in the vadose zone transforms rainfall $\delta^{18}O$ variability to cave dripwater $\delta^{18}O$ with residence times of 3 to 18 months. We observe coherent interannual dripwater $\delta^{18}O$ variability of ~3 to 5‰ related to the El Niño-Southern Oscillation (ENSO), with sustained rainfall and dripwater $\delta^{18}O$ increases caused by the 2015/2016 El Niño. Evidence of non-linear behavior is observed at one of three long-term drip monitoring sites, implying a time-varying contribution from a longer-term reservoir. Our monitoring efforts imply that well-replicated, high-resolution stalagmite $\delta^{18}O$ reconstructions from Mulu could characterize past ENSO-related variability in regional hydroclimate.

2.1 Introduction

Stalagmite oxygen isotope reconstructions provide key insights into past terrestrial hydroclimate variability from across the globe on seasonal to orbital timescales. In some tropical and subtropical regions where rainfall is dominated by strong vertical convection and infrequent year-round temperature variability, the 'amount effect' framework aids interpretations of stalagmite oxygen isotope ($\delta^{18}O_{stal}$) records. Modern empirical observations classify the 'amount effect' as a correlation between high (low) rainfall rates

on monthly and longer time scales with depleted (enriched) rainfall $\delta^{18}O$ (Craig, 1961; Dansgaard, 1964; Rozanski et al., 1993). Using the amount effect framework, overlapping $\delta^{18}O_{stal}$ records from monsoon-vulnerable regions in South America (Cheng et al., 2013; Cruz et al., 2005), Australia (Griffiths et al., 2009), Oman (Burns et al., 1998), and India (Sinha et al., 2005) demonstrate interhemispheric anti-phasing in $\delta^{18}O$ variability from precession-driven (~19 – 23ky) orbital forcing. North Atlantic millennial-length Dansgaard-Oeschger (Dansgaard et al., 1993) and Heinrich events (Heinrich, 1988) are mirrored in far-off tropical-subtropical stalagmite records that use the amount effect framework from central South America (Wang et al., 2006), China (Wang et al., 2001), and Northern (N.) Borneo (Partin et al., 2007) suggest a link between high-latitude temperature variations and changes in the monsoon (Cheng et al., 2012). Other reproducible $\delta^{18}O_{stal}$ records from N. Borneo (Carolin et al., 2013; 2016; Meckler et al., 2012; Partin et al., 2007) suggest forced changes in Walker circulation properties in the west Pacific warm pool (WPWP), a major source of heat and water vapor for the climate system across interannual timescales (e.g. the El Niño-Southern Oscillation (ENSO)) (Rasmusson and Wallace, 1983). However, to tease apart external and internal climate forcings over higher-frequency natural climate phenomenon, such as ENSO, requires sub-annually resolved $\delta^{18}O_{stal}$ records.

Improved laboratory and sampling techniques over the last twenty years allow for sub-annual to annual resolution in absolutely-dated stalagmite $\delta^{18}O$ records. Successful efforts from highly-resolved stalagmite $\delta^{18}O$ records spanning the late Holocene have identified individual tropical cyclones in Belize (Frappier et al., 2007) and Australia (Nott et al., 2007), intraseasonal variation of monsoonal rainfall in Thailand (Cai et al., 2010),

annual-length droughts in the Yucatan Peninsula (Medina-Elizalde et al., 2010), and the 1997/1998 El Niño event from a China stalagmite (Liu et al., 2018). In regions where monsoon strength is linked with the opposing cold (La Niña) and warm (El Niño) ENSO phases that occur on interannual timescales, highly-resolved $\delta^{18}O_{stal}$ records have successfully characterized precipitation-related anomalies from SE China (Zhang et al., 2018) and N. Thailand (Muangsong et al., 2014), and within the Central American countries of Panama (Lachniet et al., 2004), Belize (Akers et al., 2016), and Mexico (Lachniet et al., 2012). Long-term trends in reduced ENSO variability during the mid-Holocene were reconstructed from a N. Borneo $\delta^{18}O_{stal}$ record, but only across shorter sub-annually resolved time intervals (Chen et al., 2016). To confidently disentangle the climate signal from other local factors in $\delta^{18}O_{stal}$ reconstructions, scientists have long-since turned towards modern monitoring of rainfall, soil waters, and cave dripwaters at individual paleoclimate sites.

Long-term rainfall and cave dripwater monitoring identifies the large-scale and local influences on cave dripwater $\delta^{18}O$ variability through time. Empirical monitoring data is generalized for usage in forward proxy system models (Dee et al., 2015; Partin et al., 2013b) an effective tool that quantifies the expected variability in stalagmite $\delta^{18}O$ given a specific climatic or environmental forcing. Because stalagmite $\delta^{18}O$reconstructions reflect amount-weighted dripwater $\delta^{18}O$variations, it is important to quantify the high frequency (daily to intraseasonal) as well as lower frequency (interannual to sub-decadal) controls on rainfall and cave dripwater $\delta^{18}O$ variability at a stalagmite $\delta^{18}O$reconstruction site. For rainfall $\delta^{18}O$variability, the amount effect remains an interpretative framework for tropical $\delta^{18}O_{stal}$ records (Lachniet et al., 2004; 2009), but many studies document a range of

additional local-scale controls on modern rainfall $\delta^{18}O$ (hereinafter $\delta^{18}O_R$). In the tropics, influencing hydroclimate processes over rainfall $\delta^{18}O$ composition include upstream rainout (Konecky et al., 2019), moisture source convergence (Cai and Tian, 2016), and precipitating cloud type (Aggarwal et al., 2016). Once the rainwater falls to the ground, evaporative enrichment may alter the $\delta^{18}O_R$ signal as it infiltrates into the karst zone (Cuthbert et al., 2014). Further karst complexities that alter the $\delta^{18}O_R$ signal include the amount of reservoir or aquifer stores in the vadose zone (Ford and Williams, 2013), whether recharged waters mix with vadose waters of differing isotopic compositions (Fairchild et al., 2006), and preferred recharge flow pathway (Fairchild and Baker, 2012). Karst water flow routing varies widely, with a wide range of water transit times implied by observational data, manifest as large differences in year-to-year cave dripwater $\delta^{18}O$ (hereinafter $\delta^{18}O_D$) variability within the same cave (Partin et al., 2013a; Treble et al., 2013; Zhang and Li, 2019). Indeed, modern monitoring of rainfall and cave dripwaters remain crucial to quantify the robustness of the climate-to-calcite isotopic relationship at individual paleoclimate sites, especially those undergoing calibration efforts or the interpretation of highly-resolved $\delta^{18}O_{stal}$ records.

In this paper we present a daily rainfall $\delta^{18}O$ time series (2006 – 2018) paired with the world's longest tropical biweekly dripwater $\delta^{18}O$ time series (2007 – 2018). This study builds on monitoring work presented by Moerman et al. (2013, 2014), where vadose zone mixing translates ENSO-related variations in $\delta^{18}O_R$ to three monitored cave $\delta^{18}O_D$ sites. Using two simple modeling techniques directly related to the local $\delta^{18}O_R$ record, we estimate Mulu residence time to fall between 3 to 18 months. The ENSO-related variations in cave $\delta^{18}O_D$ observed by Moerman et al. (2014) were only quantified across one singular

El Niño and two La Niña events. Our extended sampling interval contains the very strong 2015/2016 El Niño event, which provides a strong signal to further constrain the rainfall-to-dripwater $\delta^{18}O$ transformation across the three cave $\delta^{18}O_D$ time series at our site.

2.2 Methods

2.2.1 Cavity Ring-Down Spectroscopy

All rainfall and cave dripwater samples were measured for $\delta^{18}O$ and $\delta^{2}D$ using a wavelength-scanned cavity ring-down spectrometer (WS-CRDS) (Picarro L2130-i water isotope analyzer). Picarros are fully automated trace gas analyzers using optical absorption spectroscopy of targeted gases to determine the isotopic composition of samples. Nearly all small gas-phase molecules and their isotopologue (H_2O: $^{1}H^{2}D^{18}O$, $^{1}H_2{}^{16}O$, $^{2}D^{18}O$…etc.) absorb near-infrared light at specific wavelengths, the magnitude of absorption analogous to (i) the concentration of these small molecules in a sample and (ii) the sample path length, or the distance of light that travels through a sample. The WS-CRDS has a single-frequency laser filling the sample cavity with laser light onto angled mirrors, effectively increasing sample path length. A small amount of light leaks onto a photodetector whose signal is directly equivalent to the intensity of light. The laser is on for only microseconds, yet light within the cavity bounces around the mirrors until all light has escaped, translating to the light read by the photodetector to decrease with time. The exponential decay of detectable light measured in real time is referred to as the 'ring-down', transforming optical loss into a time measurement. The machine resolves the absorption intensity of a particular wavelength by comparing the ring-down time of a cavity with gas versus an empty cavity. It continuously measures and compares the two ring-down times determining absorption

intensities, with isotopic concentrations equivalent to absorption peak height with respect to a baseline absorbance.

Precision for our Picarro L2130-i water isotope analyzer spans ± 0.1‰ and ± 0.5‰ for $\delta^{18}O$ and $\delta^{2}D$, respectively (1σ). Rainfall and cave dripwater samples were calibrated against three internal laboratory standards (heavy, intermediate, and light ($\delta^{18}O$: 5.2‰, –4.3‰, –16.4‰ respectively)) and ($\delta^{2}D$: 3.9‰, –23.7‰, –98.6‰ respectively). The internal standards were standardized using three internationally certified external standards NIST-GISP, NIST-VSMOW, NIST-SLAP. Each run has 36 samples total (147 injections), with a full suite of internal standards measured at the beginning and end of each analysis, with the intermediate standard measured after every 9th sample.

2.2.1.1 Sampling and isotopic analysis for rainfall and cave dripwaters

This study extends one rainfall and three cave drip water time series first presented by Moerman et al. (2014) from Gunung Mulu National Park in N. Borneo (4°06'N, 114°53'E). For a detailed description of the geologic and climatic setting of Gunung Mulu, the reader is referred to Cobb et al. (2007), Moerman et al. (2013), and Carolin et al. (2016). Rainfall samples were collected by Mulu Airport Meteorological staff using a splayed-bottom, copper rain gauge (Casella model M1144003). Rainfall and cave drip water samples were collected and stored in 3 mL glass vials and sealed with rubber stoppers and aluminum crimp-tops to reduce evaporation prior to analysis. All samples were measured for $\delta^{18}O$ and δD using a Picarro L2130-i cavity ring-down water isotope analyzer, with a long-term precision better than ± 0.1‰ and ± 0.5‰ (1σ, $N > 500$), respectively.

Cave dripwater samples reflect two distinct sampling strategies: (1) quasi bi-weekly collection at three established drip sampling sites by park staff (Figure 1) and (2)

collections spanning most of the Mulu formation conducted during large field expeditions (Figure 1). For each dripwater collection, corresponding drip rates were recorded in drips per minute (dpm). Time series drips Wind Fast (WF) and Wind Slow (WS) are located ~75m from the entrance to Wind Cave, roughly ~20m apart (Figure S1), dripping at 32 ± 7 dpm (1σ) 7 ± 1 dpm (1σ; Figure 5d). Time series drip L2 is located ~140m from the entranced to Lang's Cave, which is approximately 5km south of Wind Cave, dripping at 15 ± 3 dpm (1σ; Figure 5d). All three dripwater time series contain two significant sampling hiatuses: Feb-July, 2014 and Sep, 2014-Aug, 2015. Spatial surveys of stalagmite and non-stalagmite forming drip waters were collected during field expeditions in Aug, 2008 (N = 63), Feb/Mar, 2010 (N = 128), Oct/Nov 2012 (N = 291), Feb/Mar 2013 (N = 37), May, 2016 (N = 92), May, 2017 (N = 180), and Mar/Apr, 2018 (N = 124) (Figures 4, S3, S4). Lastly, Onset HOBO humidity and temperature loggers were deployed inside one of the nearby cave systems (Drunken Forest, Figure 1) in the field in 2012, measuring almost constant 100% relative humidity and 75°F from 2012 to 2015.

2.2.2 Proxy System Models

Two proxy system models were used to model the transformation of $\delta^{18}O_R$ to $\delta^{18}O_D$, generating estimates of karst residence times (τ) at Mulu. The autogenic recharge model (hereinafter called ARM) is the simplest model, creating an ensemble of modeled dripwater time series' through a backwards projected running mean of averaged daily amount-weighted local $\delta^{18}O_R$ at different weekly-averaging windows (set at 1 to 85 weeks). The bivariate mixing model (hereinafter called BMM) assigns two reservoirs (A and B), with differing $\delta^{18}O$ compositions, to feed cave drips. BMM offers a conceptual framework for aquifer mixing and allows the user to simply change contribution

percentages from each reservoir without sacrificing karst residence time. The equation for BMM is outlined below:

$$\mathbf{X_M = X_A(1 - f_B) + X_B f_B} \quad (4)$$

X_A and X_B are the isotopic composition of reservoir A and B and f_a and f_B are the reservoir A and B mixing parameters, respectively. The isotopic composition of reservoir A (X_A) was assigned as L2's modeled τ from ARM at 42 weeks and reservoir B (X_B) as the amount-weighted local $\delta^{18}O_R$ mean. Two mixing scenarios are considered in this study and were the best modeled estimations to capture L2 observations: (1) 40% contributions from reservoir A (f_b =0.6) and 60% from reservoir B (referred to as 40:60) and (2) 80% contributions from reservoir A (f_b = 0.2) and 20% from reservoir B (referred to as 80:20). For further information concerning model details of ARM and BMM, the reader is referred to Moerman et al. (2014).

2.2.3 Characterization of ENSO events

El Niño and La Niña events are characterized by NOAA's Oceanic Niño Index (ONI). El Niño (La Niña) events are defined by sea surface temperature anomalies (SSTa) in the Niño 3.4 region (5°N – 5°S, 170°W – 120°W) from ERSSTv5 remaining ≥ 0.5°C (≤ –0.5°C) for five consecutive 3-month running mean periods. The strength of events are defined by the following thresholds: weak (0.5 – 0.9 °C SSTa), moderate (1.0 – 1.4 °C), strong (1.5 – 1.9 °C), or extreme (≥ 2.0 °C). Data was accessed from https://origin.cpc.ncep.noaa.gov/products/analysis_monitoring/ensostuff/ONI_v5.php.

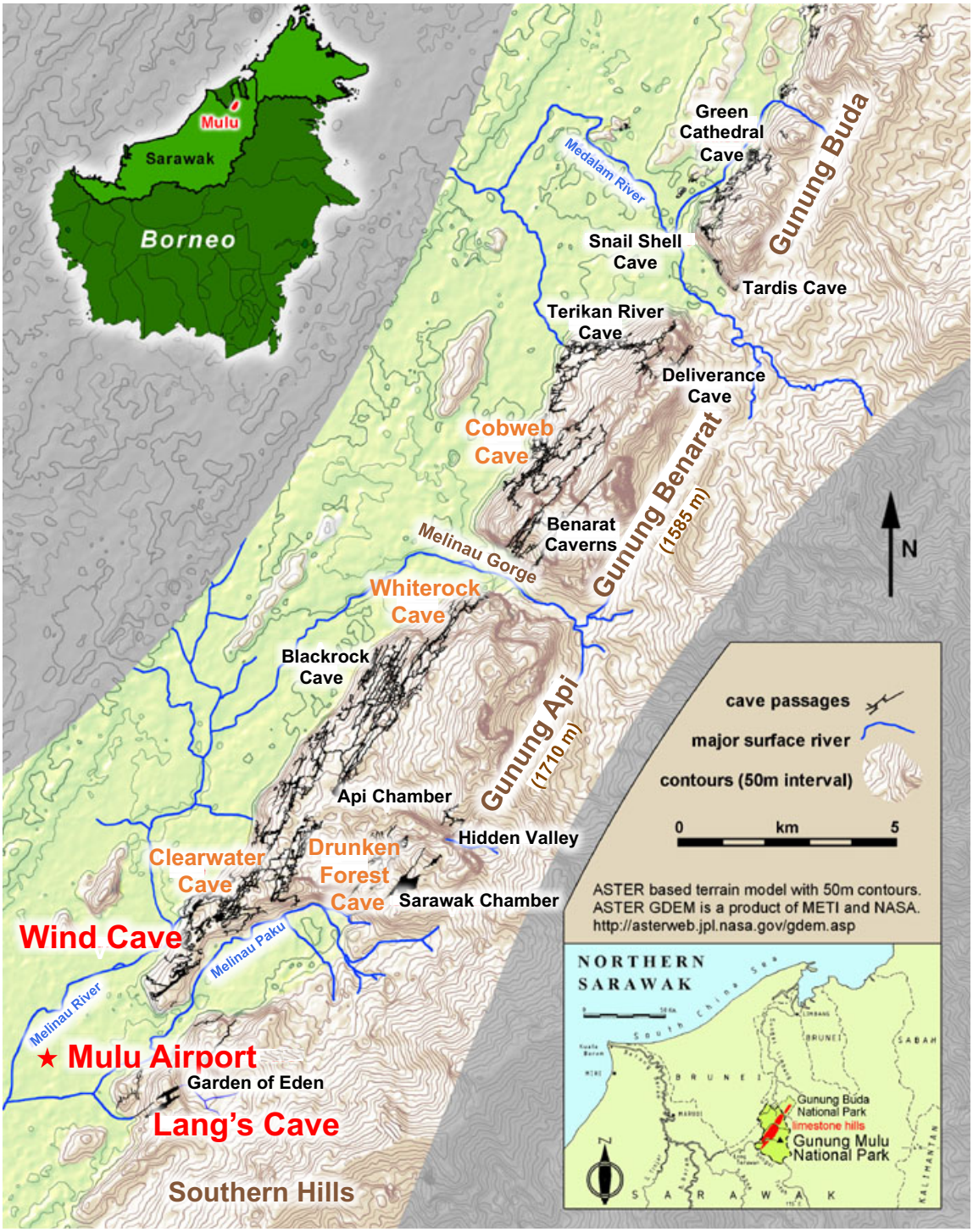

Figure 1 | Detailed map of Gunung Mulu National Park. Map on left adapted from Mulu Caves Project, with permission from Jerry Wooldridge that outlines Gunung Mulu National Park in Northern Sarawak, Borneo. The three cave dripwater and rainfall time series locations are in red, caves from seven spatial surveys of stalagmite and non-stalagmite forming drips written in orange, non-surveyed caves in black, mountains and gorges in brown, and rivers in blue.

2.3 Results

2.3.1 Diurnal to seasonal rainfall variability at Mulu

Diurnal $\delta^{18}O_R$ values vary significantly across the 12-yr time series, ranging from -1.6 to -24.3‰ (Figure 5b) with an average of -7.3 ± 3.7‰ (1σ, N = 2,664), and δD ranges from -85.4 to -153.8‰ with an average of -45.6 ± 29.6‰ (1σ, not pictured). Diurnal rainfall amount ranges from 0 to 300.3 mm/day (Figure 5e) averaging 13.8 ± 22.4 mm/day. Daily Mulu $\delta^{18}O_R$ values are significantly correlated to locally averaged rainfall and outgoing longwave radiation integrated over the previous 5 to 8 days (Figure S2a), in line with previous estimates of the water vapor residence times Mulu (Moerman et al., 2013). We observe the strongest relationship between these Mulu $\delta^{18}O_R$ and Mulu rainfall when both variables are averaged over monthly timescales (Figures S2b, Table S1). Consistent with previous studies, we observe no statistically significant difference in seasonal rainfall or $\delta^{18}O_R$ ($JAS_{2007-2017}$ = -7.5 ± 1.5 ‰ vs. $JFM_{2007-2017}$ = -6.1 ± 2.2‰; Moerman et al., 2013; Kurita et al., 2018).

2.3.2 Local Meteoric Water Line

To investigate the isotopic characterization of local meteoric waters, six different LMWL linear equations were generated from ~11 years of diurnal resolved rainfall $\delta^{18}O$ and $\delta^{2}D$ data. Figure 2 shows three different regression methods (major axis regression (MA), reduced major axis regression (RMA) and ordinary least squares regression (OLSR)), and their corresponding precipitation weighted (PW) regressions. During an extensive study generating LMWL's at 288 sites, RMA and PWRMA regression were better suited for coastal sites and oceanic islands (Crawford et al., 2014). Thus, it is unsurprising to find that the RMA and its corresponding PW regression (PWRMA) provide

best fits for our site, resulting in the lowest calculated sum of squared errors ($rmSSE_{av}$) value (RMA = 1.0015, PWRMA = 1.0014). The $rmSSE_{av}$ value is an indicator for the best regression method, with higher significance for measured values closer to 1.0 (Crawford et al., 2014). All regression methods, and corresponding PW, fall very close to the GMWL, suggesting limited local post-condensation evaporation.

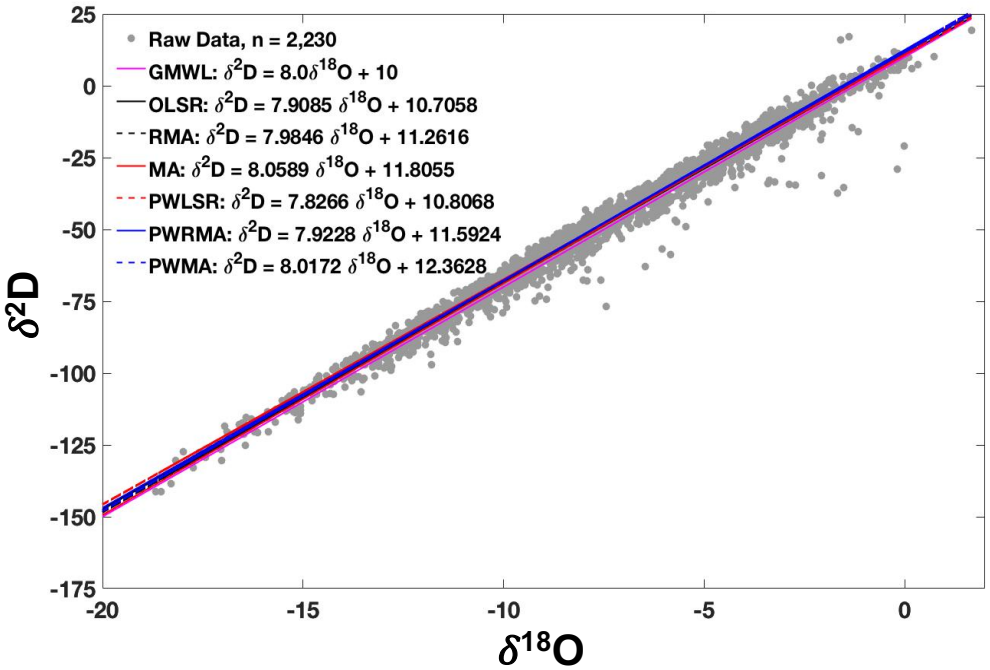

Figure 2 | Daily rainfall $\delta^{18}O$ vs. $\delta^{2}D$ from Mulu. N. Borneo daily rainfall $\delta^{18}O$ versus $\delta^{2}D$ for 11-year time series (grey circles). The dashed lines are linear fits for the 11-year time series from three different regression methods and their corresponding precipitation weighted regressions. Methodology used for each regression line is outlined in detail in *Crawford* (2014) and was generated using a LMWL model provided by the Australian Nuclear Science and Technology Organisation with permissions from Dr. Niels Munksgaard.

2.3.3 Rainfall $\delta^{18}O$ variability across ENSO extremes

ENSO is the dominant driver of rainfall $\delta^{18}O$variability in N. Borneo, where individual El Niño and La Niña events influence diurnal to interannual $\delta^{18}O_R$ variability, in line with previous studies (Kurita et al., 2018; Moerman et al., 2013; Tangang et al., 2017). Over the entire dataset, $\delta^{18}O_R$ is correlated to ENSO (e.g. Niño 4 SSTa), which explains up to ~26% of total monthly variance. With respect to individual events, the

2009/10 and 2015/16 El Niño events included ~50 and 90 days, respectively, of significantly enriched $\delta^{18}O_R$ during JFM (> +2.2 per mil from the long-term JFM mean; Figure 3). The 2007/08 and 2010/11 La Niña events had ~30 days of significantly depleted rainfall $\delta^{18}O$ during JFM with a larger isotopic spread (Figure 3). On seasonal timescales, $\delta^{18}O_R$ is significantly correlated to a range of ENSO indices summarized in supplementary Table 2 (e.g. R($\delta^{18}O_R$, Niño 3)=0.58, R($\delta^{18}O_R$, Niño 4=0.64); p<0.01). Conversely, local rainfall amount, exhibits lower correlations to ENSO indices (e.g. R($\delta^{18}O_R$, Niño 3= -0.26, R($\delta^{18}O_R$, Niño 4= -0.35); p<0.01) (Table S2).

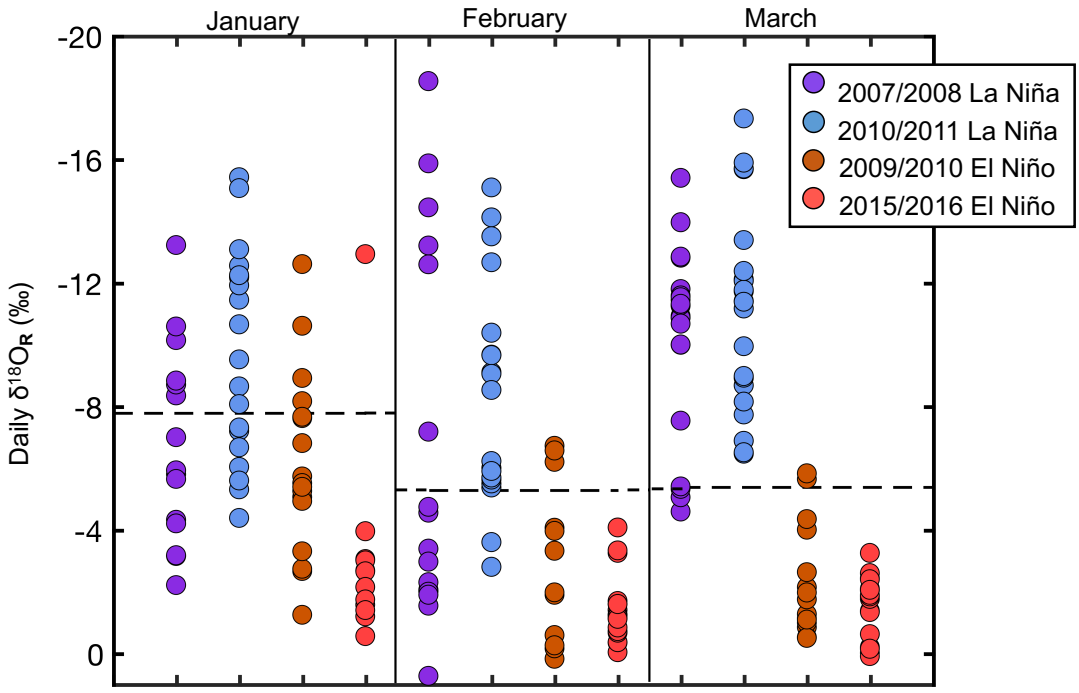

Figure 3 | Spread of Mulu daily rainfall $\delta^{18}O$ in January, February and March (JFM) during four extreme ENSO events. Dashed lines indicate the respective monthly averages for the entire $\delta^{18}O$ data set (January = -7.8 ± 2.5‰; February = -5.3 ± 2.3‰; March = 5.4 ± 3.3‰). Note the JFM seasonal average for the entire rainfall time series is -6.1 ± 2.2‰. All values reported are 1σ. Y-axis is inverted.

2.3.4 Cave dripwater $\delta^{18}O$ variability as a function of local rainfall $\delta^{18}O$

Dripwater $\delta^{18}O$ values for Wind Fast and Wind Slow $\delta^{18}O_D$ range from -3.7 to –11.6‰ and -3.4 to -11.7‰, respectively, while values for Lang's Cave range from –5.9

to −10.0‰ (Figure 5c). Wind Fast (WF) and Wind Slow (WS) $\delta^{18}O_D$ values average -7.9 ± 1.3‰ (1σ, N = 253) and -7.7 ± 1.3‰ (1σ, N = 254), respectively, and L2 $\delta^{18}O_D$ average -8.1 ± 0.7‰ (1σ, N = 253). There is no clear relationship between $\delta^{18}O_D$ and drip rate, nor local rainfall and drip rate, on any timescale.

All three cave $\delta^{18}O_D$ time series display coherent interannual fluctuations driven by ENSO variability, consistent with our analysis of $\delta^{18}O_R$ variability. WF and WS drips reflect a higher range of interannual $\delta^{18}O_D$ variability (~3 to 5‰) in comparison to L2 (~1 to 2.5‰). All three $\delta^{18}O_D$ time series become more enriched (depleted) during El Niño (La Niña) events and remain so for 1 – 16 months following the peak of each event (Figure 5c and 6). The most depleted $\delta^{18}O_D$ values in all three caves occurred in December 2008, likely related to a 7-day-long period of intense, relatively depleted rainfall during October 2008 (~450mm, -12.8‰; Figure S6) driving non-stationary recharge behavior in the Mulu karst. The very strong 2015/2016 El Niño was characterized by peak SST anomalies (SSTa) during November 2015 (ERSSTv5, Niño 3 index at +2.91ºC SSTa), maximum rainfall $\delta^{18}O$ anomalies during JFM, and maximum $\delta^{18}O_D$ values in Feb 2016 for drips WF and WS (-3.7‰ and -3.4‰, respectively) and in May 2016 for drip L2 (-5.9‰). Indeed, $\delta^{18}O_D$ anomalies across all three caves scale with the size of ENSO-related SST anomalies, with the largest excursions observed during the 2015/2016 El Niño event (Figure S5). We observe a strong linear relationship between cave $\delta^{18}O_D$ and NIÑO3.4 SST anomalies at both Wind cave sites (R^2=0.94 and R^2=0.92 for WF and WS, respectively), whereby El Niño (La Niña) events correspond to enriched (depleted) cave $\delta^{18}O_D$ values. Lang's cave $\delta^{18}O_D$ values are also significantly correlated to NINO3.4 SST values (R^2=0.54, $p<0.05$), but are overall lower than the correlations observed for Wind Cave. (R^2 = 0.54) (Figure

S5).

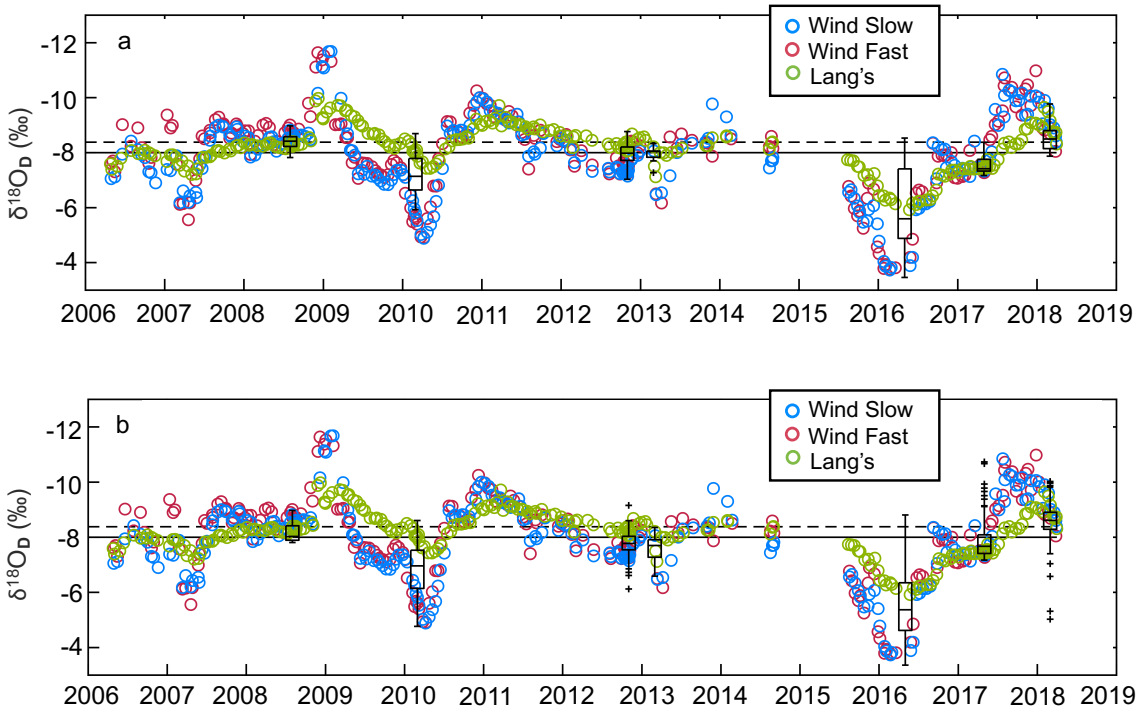

Figure 4 | Spatial cave dripwater $\delta^{18}O$ survey results against three Mulu cave dripwater $\delta^{18}O$ time series. Cave dripwater $\delta^{18}O$ observations denoted in colored circles from Wind Fast (WF, maroon), Wind Slow (WS, blue), and Lang's cave (L2, green). In both panels, boxes denote the 25 – 75% quartile range of surveyed cave dripwater $\delta^{18}O$ and whiskers as $\pm 2.7\sigma$ of distributed expedition data and outliers as any values outside of this standard deviation (black crosses). Mulu's amount-weighted rainfall $\delta^{18}O$ is denoted as a dashed line (-8.4 ± 2.4‰) and the combined mean from all three cave dripwater $\delta^{18}O$ time series as a solid line (-8.0 ± 1.2‰) in panels a and b. The standard deviation is reported as 1σ. (a) Stalagmite-forming and (b) non-stalagmite forming cave dripwater $\delta^{18}O$ during each survey as box and whisker plots. Y-axes are inverted in both panels.

Seven spatial surveys of stalagmite and non-stalagmite forming cave $\delta^{18}O_D$ from nine cave systems reflected system-wide shifts in $\delta^{18}O_D$ associated with ENSO variability. During the largest events (2010 and 2015/2016 El Niño), cave-wide $\delta^{18}O_D$ values exhibited the most spread, as drips with a faster residence time reflected large $\delta^{18}O_R$ anomalies during these times, while some reflected little if any shift from long-term average $\delta^{18}O_D$, possibly indicative of multi-year residence times (Figure S4). We observed no significant difference

in $\delta^{18}O_D$ mean values for stalagmite-forming versus non-stalagmite-forming drips (-7.8 ± 0.8‰ (1σ, N = 356) and -7.5 ± 1.1‰ (1σ, N = 577), respectively (Figure 4, S3).

2.3.5 Estimates of Mulu karst residence times

Modeled $\delta^{18}O_D$ time series employ local rainfall $\delta^{18}O$ to quantify residence times for the three dripwater $\delta^{18}O$ time series, capturing up to 85% of the observed dripwater $\delta^{18}O$ variability. The autogenic recharge model (ARM) tracks the variability for $\delta^{18}O_D$ observations at WF and WS using residence times of 18 weeks (R_{WF}=0.89, R_{WS} = 0.93 ($p<0.05$), Figure 6a). With a residence time of 42 weeks, ARM provides a reasonable fit to L2 $\delta^{18}O_D$ observations ($R=0.85$, $p<0.05$; Figure 6b; Table S3), but significantly overestimates the amplitude of $\delta^{18}O_D$ variations by ~ +/- 1‰.

A bivariate mixing model (BMM) that employs two reservoirs – a fast-responding and a slow-responding reservoir - provides a better fit to the L2 $\delta^{18}O_D$ observations relative to the single reservoir model. To determine the ratio of the reservoirs that best matches the observed L2 $\delta^{18}O_D$ time series, we define a short-term reservoir A (assigned a residence time of 42 weeks, see above) and longer-term reservoir B (assigned a value of -8.4‰, which reflects the amount-weighted mean the $\delta^{18}O_R$ time series). Conceptually, reservoir A represents 'newer' water contributions from recharged rainfall while reservoir B simulates an older, well mixed reservoir of vadose waters. Two mixing scenarios are considered in this study as the best modeled estimations to capture L2 observations: (1) 40% contributions from reservoir A and 60% from reservoir B (hereafter referred to as "40:60") and (2) 80% contributions from reservoir A and 20% from reservoir B (hereafter referred to as "80:20"). The 40:60 mixing scenario yields a significant improvement on the ARM (Table S3; $R=0.86$, $p<0.05$), particularly during the 2009/2010

El Niño event, and during an ENSO-neutral period from 2012 – 2014 (Figure 6b, purple line). The 80:20 mixing scenario also improves on the ARM (Table S3; R = 0.86, $p<0.05$), particularly the strongly enriched (depleted) isotopic excursions associated with large El Niño (La Niña) anomalies (Figure 6b, pink and maroon lines).

An analysis of correlation coefficients and residuals between the modelled and observed dripwater $\delta^{18}O$ values for L2 finds an optimal fit when the residence time for reservoir A changes from 42 weeks during 2007 – 2014 to 67 weeks during the period 2015 – 2018 (Figure 6b, Table S3). Such a large change in L2 residence time is indicative of non-stationary karst behavior. Non-stationary behavior in the L2, WF, and the WS cave $\delta^{18}O_D$ time series was previously observed by Moerman et al., (2013) most likely driven by heavy rainfall events in October 2008, given the simple ARM could not capture anomalously depleted cave $\delta^{18}O_D$ observations. However, the distribution of rainfall event intensity during the 2015-2018 periods are not statistically distinguishable (Figure S6), implying that recharge rates were not the underlying cause of the abrupt change in mixing scenarios (from 40:60 to 80:20) and residence times (42 weeks to 67 weeks) during this period at Lang's Cave. Rather, we hypothesize that four consecutive seasons of enriched $\delta^{18}O_R$ ($\leq$ -5.0‰) during July 2015 to April 2016 period may have delayed the dripwater $\delta^{18}O$ recovery from the 2015/2016 El Niño event at Lang's Cave,

extending enriched dripwater $\delta^{18}O$ values through the ensuing La Niña event in 2016/17 (Figure 6b).

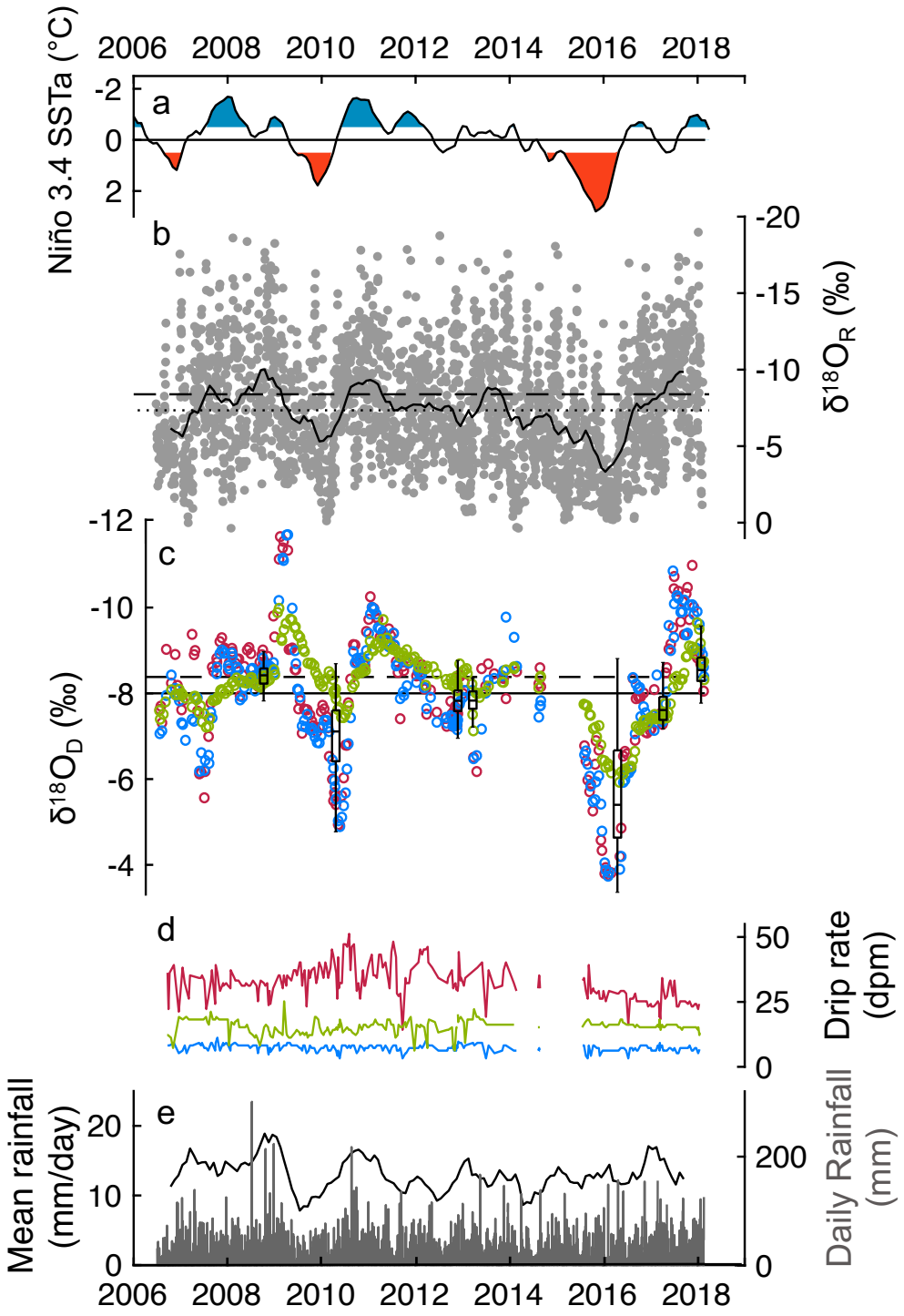

Figure 5 | N. Gunung Mulu rainfall and cave dripwater oxygen isotope time series. (a) Niño 3.4 SSTa index (ERSSTv5, Huang et al., 2017), plotted as a 3-month running average.

Red (blue) coloring indicates warm (cold) ENSO anomalies based on a threshold of +0.5ºC (–0.5 ºC). (b) Mulu daily rainfall $\delta^{18}O$ (grey circles, non-amount-weighted) plotted with a 7-month running mean (black line). Non-amount weighted average $\delta^{18}O_R$ for the entire time series is indicated by a dotted line (-7.3 ± 3.7‰) while the amount-weighted average $\delta^{18}O_R$ is indicated by a dashed line (–8.4 ± 2.4‰). (c) Mulu cave $\delta^{18}O_D$ from Wind Fast (WF; maroon circles), Wind Slow (WS; blue circles), and Lang's Cave (L2; green circles). The solid line indicates the $\delta^{18}O_D$ averaged across all three drips (–8.0 ± 1.2‰), while the dashed line represents the amount-weighted $\delta^{18}O_R$ average plotted in (b). Box (25^{th}-75^{th} quartiles) and whiskers (total range, excluding outliers, see Figure 4) represent $\delta^{18}O_D$ values from 7 spatial drip surveys. (d) Drip rate in drips per minute (dpm) for the three time series drips plotted in (c), plotted in the corresponding color. (e) Daily Mulu rainfall amount (grey bars) plotted with the 7 month running average (solid black line). Y-axes in panels A, B, and C are inverted. Monthly ERSSTv5 data found online at https://www.cpc.ncep.noaa.gov/data/indices/ersst5.nino.mth.81-10.ascii. All standard deviation values are reported to 1σ.

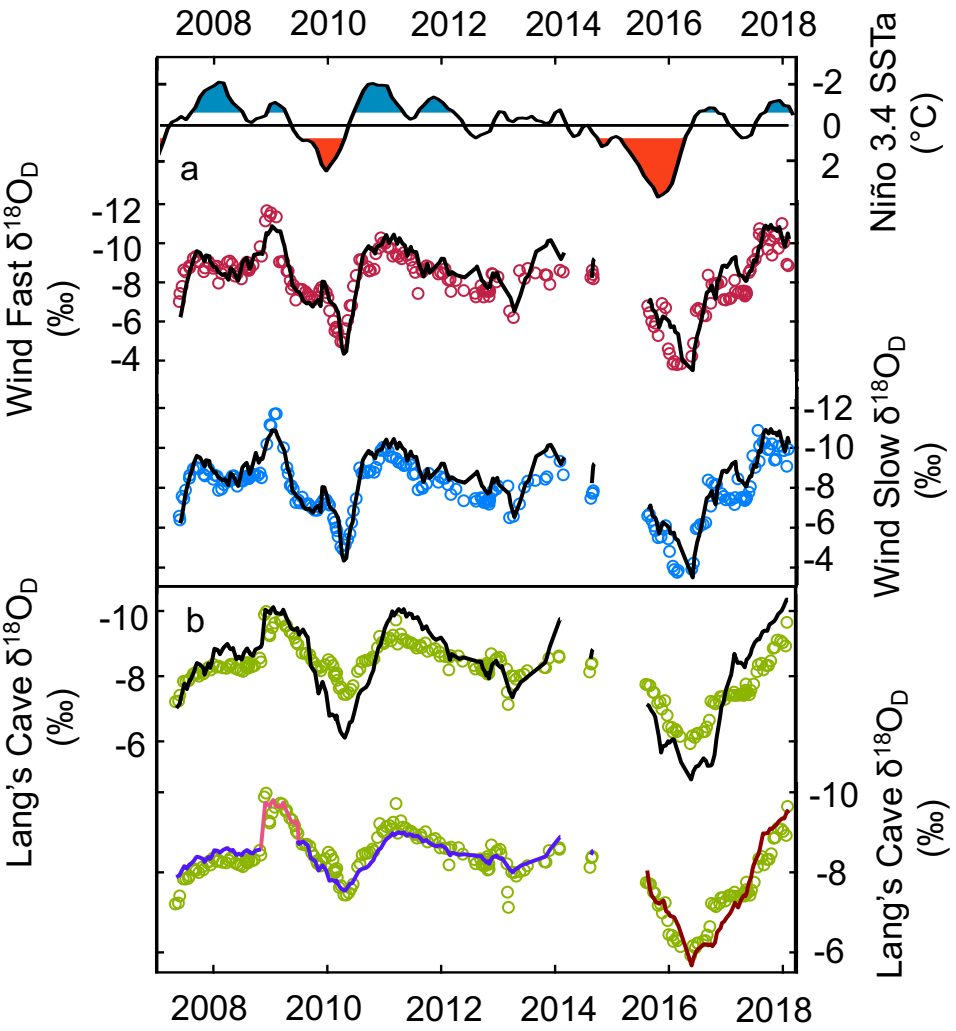

Figure 6 | Observed versus modeled Mulu dripwater $\delta^{18}O$ time series. (a) The top panel is NIÑO3.4 SSTa index (ERSSTv5, Huang et al., 2017), plotted as a 3-month running average. Red (blue) coloring indicates warm (cold) ENSO anomalies based on a threshold of +0.5ºC (–0.5 ºC). Observed (open circles) and modeled (black line) $\delta^{18}O_D$ for drips Wind Fast (WF; maroon) and Wind Slow (WS; blue) using a residence time of 18 weeks from the autogenic recharge model. (b) Observed (open circles) $\delta^{18}O_D$ for Lang's Cave (L2; green). The top panel shows modeled $\delta^{18}O_D$ (black line) using a residence time of 42 weeks from the autogenic recharge model. The bottom panel shows $\delta^{18}O_D$ from the bivariate mixing model (dual-reservoir). For pink and purple (maroon) lines, residence time selected is 42 weeks (67 weeks). Reservoir A=42 or 67 weeks from the autogenic recharge model and Reservoir B is the Mulu amount-weighted rainfall $\delta^{18}O$ mean (-8.4‰). An A:B mixing ratio of 40:60 (purple line) and an A:B mixing ratio of 80:20 (pink and maroon lines) provide an optimal data fit. Note that y-axes are inverted in all panels and different y-axes scalings.

2.4 Discussion

Interannual variations from ENSO-driven rainfall $\delta^{18}O$ are evident in all three Mulu cave dripwater $\delta^{18}O$ time series, reflecting rainfall $\delta^{18}O$ variations with karst residence times of 3 to 18 months. Indeed, all three cave $\delta^{18}O_D$ time series are consistent with a relatively simple transformation of $\delta^{18}O_R$ to cave $\delta^{18}O_D$, supporting previous descriptions of diffuse-seepage flow at Mulu (Cobb et al., 2007; Moerman et al., 2014; Partin et al., 2013a). The faster karst residence time at Wind cave (3-10 months) implies less homogenization of $\delta^{18}O_R$ and/or less vadose zone mixing with other reservoirs of karst waters, resulting in higher amplitude $\delta^{18}O_D$ variability (-3.7 to -11.7‰). This is especially evident during individual ENSO extremes. The longer karst residence times (10 – 18 months) documented at Lang's Cave result in smaller $\delta^{18}O_D$ variations (-5.9 to -10.0‰). The residence time differences between Wind and Lang's Caves are somewhat proportional to the karst overburden, whereby larger overburden at Lang's Cave relative to Wind Cave (~200 versus 100m) correlates with longer residence times. It is difficult to compare our residence time estimates with other tropical or ENSO-influenced cave $\delta^{18}O_D$ sites given that (i) most tropical cave $\delta^{18}O_D$ monitoring sites are characterized by high

rainfall seasonality and seasonal recharge (Beal et al., 2019; Fleitmann et al., 2004; Jones et al., 2000; Kennett et al., 2012; Lases-Hernandez et al., 2019; Mickler et al., 2004; Partin et al., 2012) and (ii) there are no other multi-year tropical cave $\delta^{18}O_D$ time series that capture ENSO extremes in $\delta^{18}O_D$ (Chen and Li, 2018; Sun et al., 2018; Zhang and Li, 2019).

Non-stationary behavior in the Lang's cave dripwater $\delta^{18}O$ time series reflects variable karst residence times and/or changes in mixing ratios between a fast-responding and long-term reservoir. In previous N. Borneo dripwater studies from Lang's Cave, non-stationary flow behavior in $\delta^{18}O_D$ and drip rate was observed from heavy rainfall events or prolonged drier conditions (Moerman et al., 2014; Partin et al., 2012). Hydrological extremes impact the hydraulic pressure of karst waters, potentially causing a change in drainage routes and/or aquifer storage (Ford and Williams, 2013). This type of non-stationary behavior is well-documented across a variety of latitudes and climates, including rapid infiltrations of tropical cyclone $\delta^{18}O_R$ (Lases-Hernandez et al., 2019), as well as changes to drip-rate in SE Australia from rapid infiltration events (McDonald and Drysdale, 2007), and in N. England associated with rapid snowmelt events (Baker and Brundsdon, 2003). In tropical caves, high rainfall seasonality combined with relatively short karst residence times ranging from 1 to 3 months (Jones et al., 2000; Lases-Hernandez et al., 2019) to less than 12 months (Partin et al., 2012) generate a seasonal bias in cave $\delta^{18}O_D$ variability skewed towards the $\delta^{18}O_R$ of the dominant recharge period. Indeed, Baker et al., (2019) documents this behavior across many tropical karst sites with mean annual temperatures > 16ºC. However, given that Mulu is not characterized by significant

differences in seasonal rainfall, we do not observe a seasonal bias in our cave dripwater $\delta^{18}O$ time series.

The fact that ENSO-related changes in Mulu rainfall $\delta^{18}O$ are recorded in Mulu cave dripwater $\delta^{18}O$ time series has important implications for the reconstruction of ENSO in Mulu cave stalagmite $\delta^{18}O$ records. While ENSO anomalies are apparent in drips fed by sources with residence times as long as 18 months, our results demonstrate that the amplitude of ENSO-related cave dripwater $\delta^{18}O$ variations is inversely correlated to karst water residence times. even for relatively long residence times of up to 18 months. Indeed, larger spatial surveys of Mulu cave $\delta^{18}O_D$ values during ENSO extremes demonstrates that while the distribution of cave $\delta^{18}O_D$ values shifts significantly during ENSO extremes, the amplitude of the ENSO-related cave $\delta^{18}O_D$ anomalies differs up to ~6.0‰ across the system at any one sampled time. These conclusions hold equally true for the subset of Mulu cave drips that feed actively accreting stalagmites (Figure 4). Other studies that capture individual ENSO events in rainfall, cave dripwater, soil water, and/or stalagmite $\delta^{18}O$ time series also document responses of different amplitudes (Chen and Li, 2018; Sun et al., 2018). Singular $\delta^{18}O_{stal}$ records from tropical (Fleitmann et al., 2003; Lachniet et al., 2004) and subtropical (Zhao et al., 2016; Tan et al., 2014) regions have documented rainfall variations associated with El Niño and La Niña events, where such records are found to be most useful for investigating long-term ENSO variability rather than individual events. Despite evidence presented herein that dripwater residence times may vary through time, a singular stalagmite reconstruction from Mulu inferred long-term reduced ENSO variability in the WPWP during the mid-Holocene at selected sub-annual intervals (Chen et al., 2016). Thus, best practice would dictate the use of

multiple stalagmite $\delta^{18}O$ records to yield robust reconstructions of interannual climate variability, following on the success of well-replicated stalagmite $\delta^{18}O$ records of centennial- to millennial-scale at the Gunung Mulu (Carolin et al., 2013; 2016; Partin et al., 2007; 2013a). Unfortunately, fast-growing samples capable of resolving ENSO variability are quite rare (Orland et al., 2014), such that it might be more practical to focus on assessing common trends in variance between reconstruction sites that capture a given climate phenomenon of interest. In that case, proxy system forward models (Evans et al., 2013; Dee et al., 2015) of the rainwater-to-dripwater $\delta^{18}O$ transformation at stalagmite $\delta^{18}O$ reconstruction sites would accelerate progress towards the identification and intercomparison of ENSO-related signals in a network of stalagmite $\delta^{18}O$ reconstructions.

2.5. Conclusions

Long-term monitoring of rainwater and dripwater $\delta^{18}O$ at Gunung Mulu National Park enables the quantification of karst residence times ranging from ~3 to 18-months. Simple linear transformation of amount-weighted rainfall $\delta^{18}O$ to dripwater $\delta^{18}O$ capture ~75 – 85% of the variance expressed at three drip sites in our study. ENSO extremes are associated with local rainfall $\delta^{18}O$ anomalies of ~6 - 8‰, and dripwater $\delta^{18}O$ anomalies of ~3- 5‰. Seven extensive spatial dripwater $\delta^{18}O$ surveys indicate system-wide changes in dripwater $\delta^{18}O$ related to ENSO variability, with no statistical difference between stalagmite-forming and non-stalagmite-forming cave dripwater sites. One of the three long-term drip monitoring sites exhibits nonstationary behavior in karst residence times, implying time-varying contributions from a well-mixed longer-term karst water reservoir. As such, our results suggest that while stalagmite $\delta^{18}O$ records from Gunung Mulu are

prime candidates for ENSO reconstruction, multiple stalagmite $\delta^{18}O$ records are required to assess the robustness such reconstructions. Lastly, our work demonstrates the utility of site-specific, long-term monitoring of rainfall and cave dripwater $\delta^{18}O$ to inform the climatic interpretation of stalagmite $\delta^{18}O$ records.

SUPPLEMENTAL INFORMATION

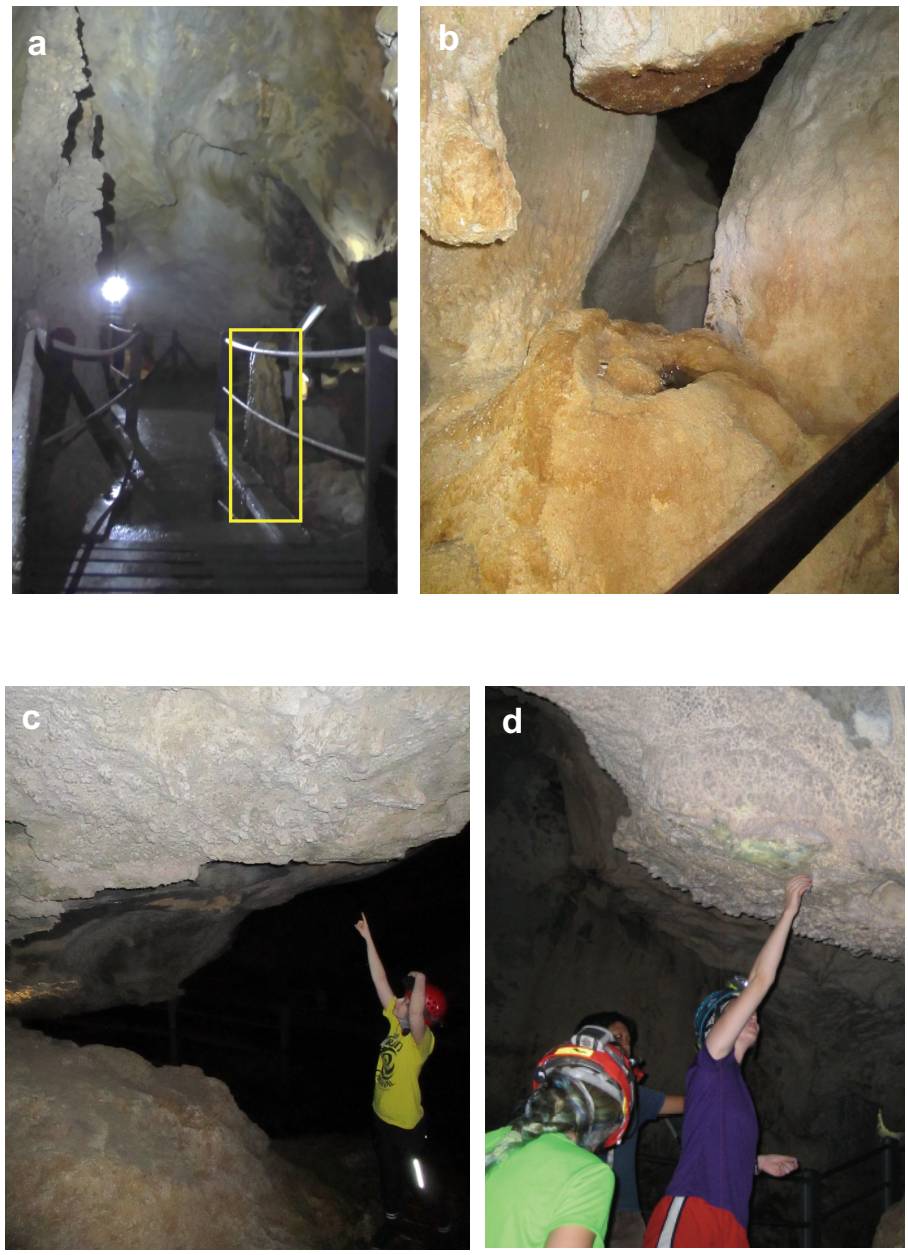

Figure S1 | Photos of cave dripwater time series sites. (a) Lang's Cave (L2), (b) Wind Fast (WF), (c) Wind Slow (WS), and (d) WS. L2 drips onto ~2m tall stalagmite, WF drips onto edge of indented pool, and WS drips onto detrital bedrock. L2 is overlain by ~200m of limestone bedrock and WF and WS by ~100m of bedrock.

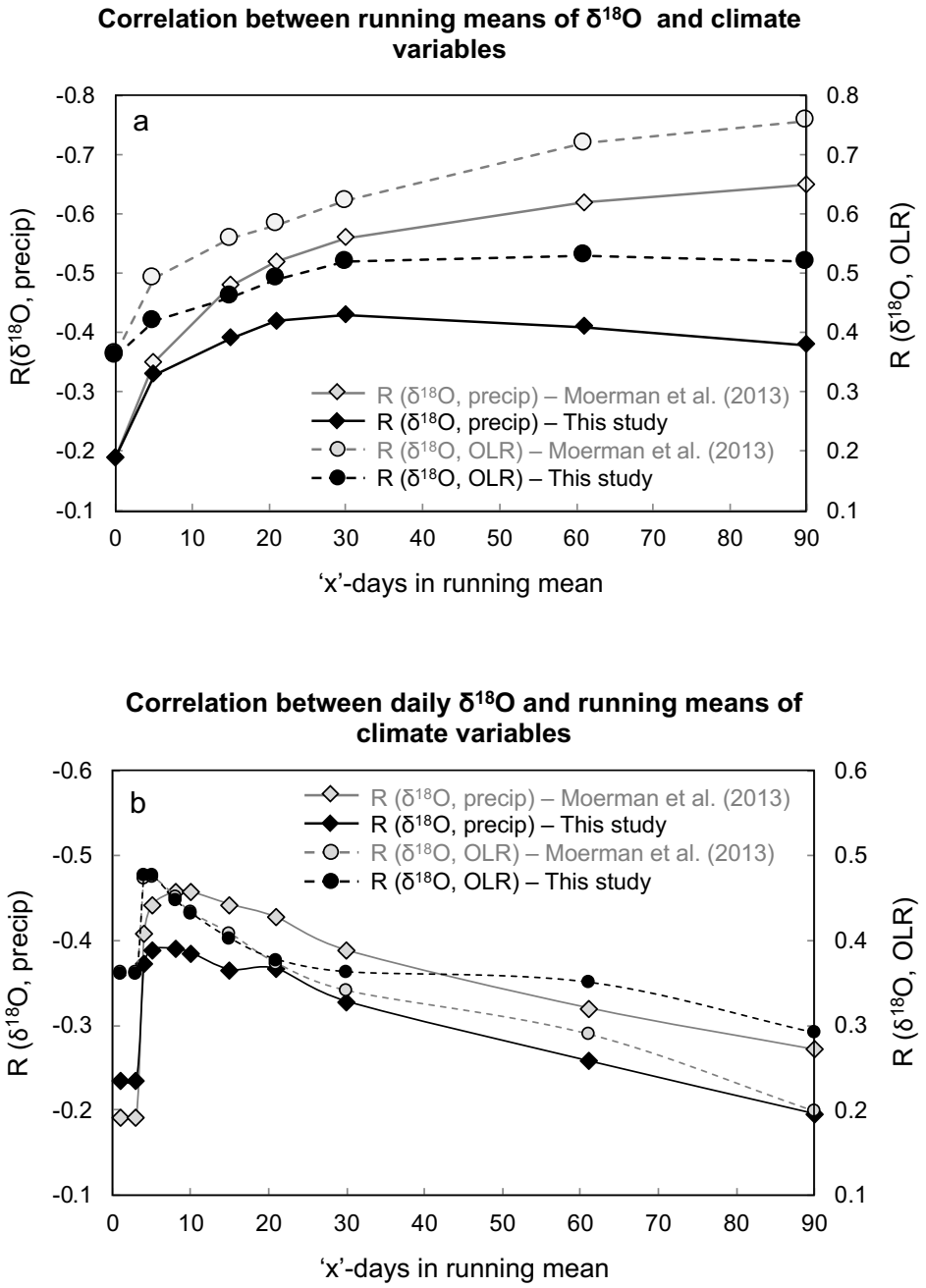

Figure S2 | Relationship between diurnal to monthly-scale variations in Mulu rainfall $\delta^{18}O$ versus local hydrological variables. (a) Correlation between 'x'-day running mean of Mulu rainfall $\delta^{18}O$ and 'x'-day running means of local Mulu precipitation amount (diamonds) and outgoing longwave radiation (OLR; circles), shown as the 2.5° x 2.5° grid box centered about 5°N, 115°E from https://www.esrl.noaa.gov/psd/data/gridded/data.interp_OLR.html. (b) Correlations between daily rainfall $\delta^{18}O$ values and 'x'-day running means of local Mulu precipitation amount (diamonds) and OLR (circles).

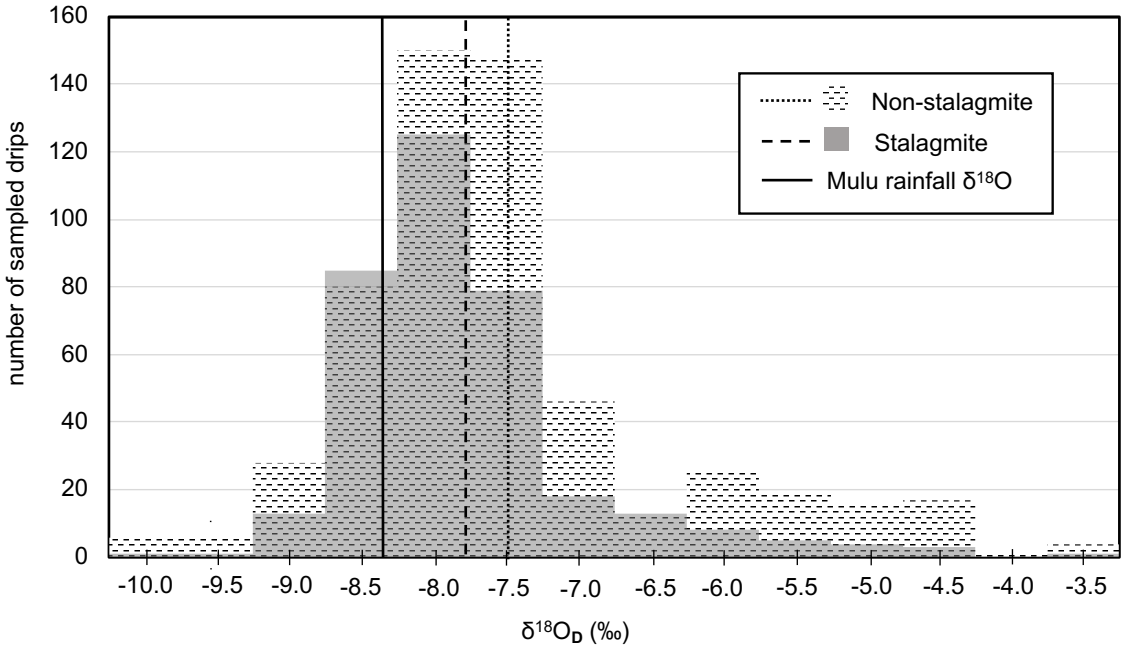

Figure S3 | Histogram of stalagmite vs. non stalagmite forming cave dripwater $\delta^{18}O$ values combined from seven spatial surveys. Non-stalagmite (stalagmite) forming drips are represented by dashed (grey) boxes and solid (dashed) lines denoting mean value and standard deviation (1σ), respectively. Non-stalagmite (N = 577) forming cave dripwater $\delta^{18}O$ mean is -7.5 ± 1.1 ‰ (1σ) and the stalagmite (N = 356) forming cave dripwater $\delta^{18}O$ mean is -7.8 ± 0.8 ‰ (1σ). Dotted line denotes the Mulu amount-weighted mean rainfall $\delta^{18}O$ (–8.4 ± 2.4‰ (1σ).

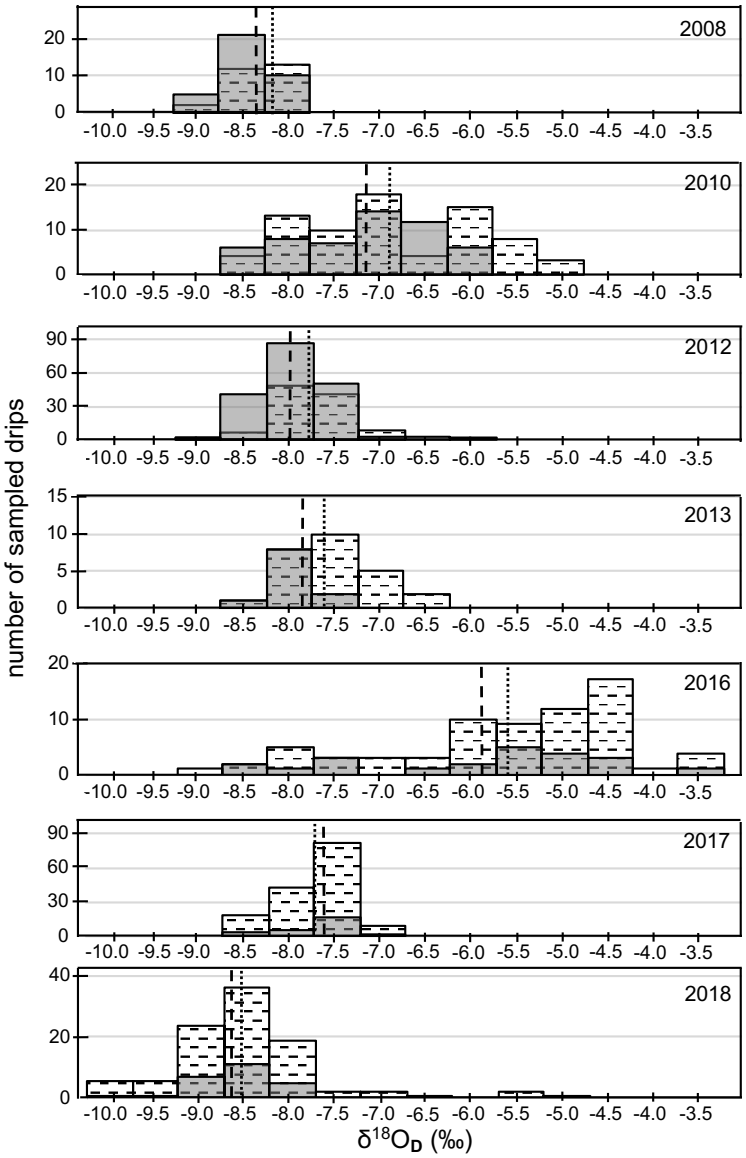

Figure S4 | Histograms from seven field spatial surveys over 2008 – 2018. Grey (dashed) boxes and dashed (dotted) lines indicate stalagmite (non-stalagmite) forming cave dripwater $\delta^{18}O$ and their corresponding mean value during each respective expedition. The y-axis displays number of sampled drips, and are different in scaling for each panel. All reported mean values are 1σ. Stalagmite forming drip means include August 2008 (-8.4 ± 1.4‰), February/March 2010 (-7.2 ± 0.7‰), October/November 2012 (-8.0 ± 0.3‰), March 2013 (-7.9 ± 0.3‰), May 2016 (-5.9 ± 1.4‰), May 2017 (-7.6 ± 0.3‰), and March/April 2018 (-8.6 ± 0.5‰). Non-stalagmite forming drip means include August 2008 (-8.2 ± 0.4‰), February/March 2010 (-6.9 ± 1.0‰), October/November 2012 (-7.8 ± 0.4‰), March 2013 (-7.6 ± 0.4‰), May 2016 (-5.6 ± 1.3‰), May 2017 (-7.7 ± 0.4‰), and March/April 2018 (-8.5 ± 0.8‰). All standard deviations are reported as 1σ.

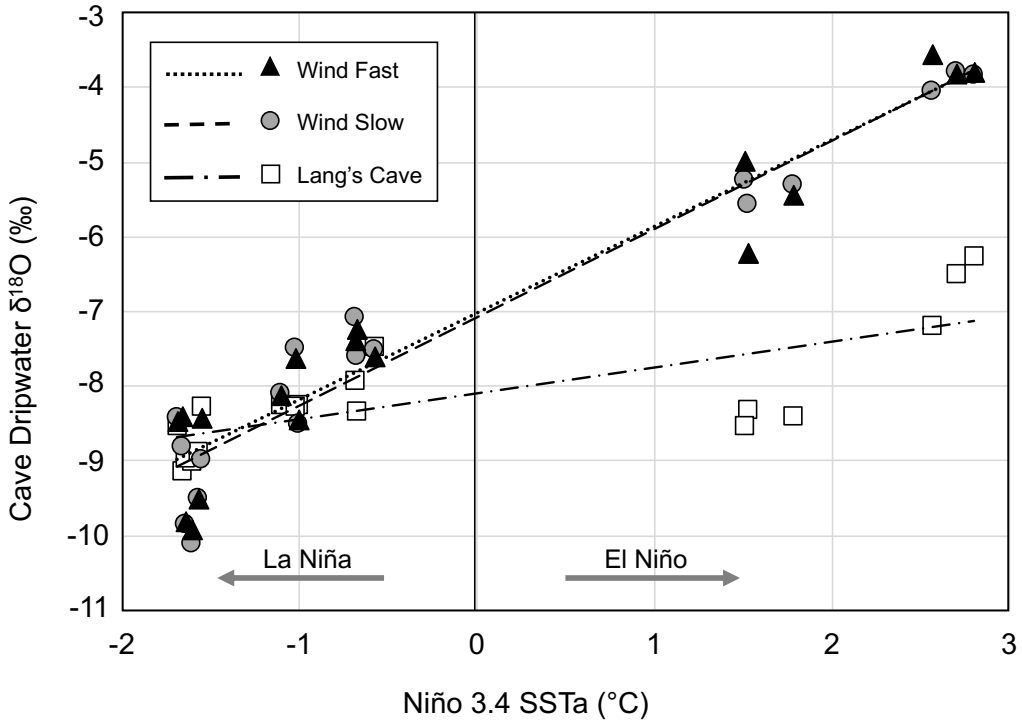

Figure S5 | Observed dripwater $\delta^{18}O$ excursions versus different ENSO events. Independent dripwater $\delta^{18}O$ observations from Wind Fast (WF, triangles), Wind Slow (WS, circles), and Lang's Cave (L2, squares) plotted against sea surface temperature anomalies (SSTa) in the Niño 3.4 region during specific time periods. Three observations were chosen at WF/WS(L2) approximately 3(10) months after the three most anomalous Niño 3.4 SSTa months, following the lag implied by the dripwater residence time calculations. Linear regressions plotted in black for WF (dotted; $R^2 = 0.94$), WS (dashed; $R^2 = 0.92$), and L2 (dash-dot; $R^2 = 0.54$).

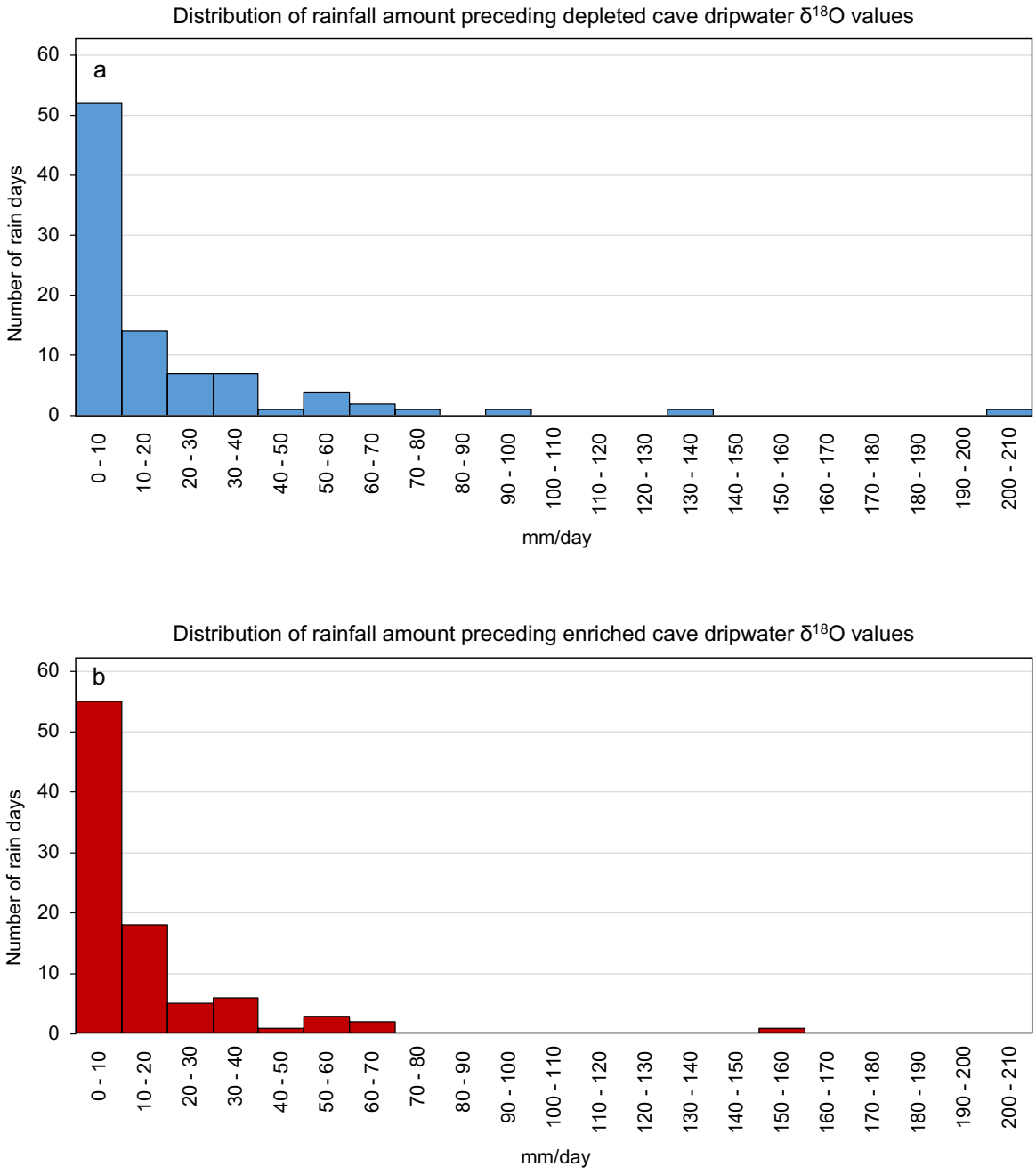

Figure S6 | Histogram comparison of potential hydraulic loading on anomalous cave dripwater $\delta^{18}O$ values. (a) Histogram of 90 days of Mulu rainfall amount (October, November, December) before anomalously depleted cave dripwater $\delta^{18}O$ observations (December 2008: Lang's Cave = -10.0‰, Wind Fast = -11.7‰, Wind Slow = -11.7‰). (b) Same as panel a, but 90 days of Mulu rainfall amount (March, April, May) before anomalously enriched Lang's Cave dripwater $\delta^{18}O$ observations in May 2016 (Lang's Cave, -5.9‰; enrichment for Wind Fast and Wind Slow occurred in February 2016 at -3.7‰ and -3.4‰, respectively).

Supplemental Table 1 | Correlations of Mulu rainfall oxygen isotopes versus rainfall amount from this study and Moerman et al. (2013). The reported correlations are plotted in Figure S3 panel a.

Mulu rainfall $\delta^{18}O$ vs. Mulu rainfall amount		
'x'-days in running mean	**Moerman et al. 2013**	**This study**
0	-0.19	-0.21
15	-0.48	-0.39
21	-0.52	-0.42
30	-0.56	-0.43
61	-0.62	-0.41
90	-0.65	-0.38

Supplemental Table 2 | Correlations with N. Borneo rainfall time series against various tropical Pacific climate indices. N. Borneo rainfall data is a 3 month centered average of each variable where $p<0.01$. All NIÑO data is from (*Huang et al.,* 2017) (ERSSTv5) found online at https://www.cpc.ncep.noaa.gov/data/indices/ersst5.nino.mth.81-10.ascii. ONI data was found online at https://www.esrl.noaa.gov/psd/data/correlation/oni.data, all SOI data found online at https://www.esrl.noaa.gov/psd/data/correlation/soi.data, and El Niño Modoki Index found online at http://www.jamstec.go.jp/frcgc/research/d1/iod/DATA/emi.monthly.txt.

ENSO Index	**Pearson's correlation coefficient ($\delta^{18}O_R$)**	**Pearson's correlation coefficient (Rainfall Amount)**
NIÑO1+2	0.46	-0.22
NIÑO3	0.58	-0.26
NIÑO3.4	0.62	-0.30
NIÑO4	0.64	-0.35
ONI	0.66	-0.28
SOI	-0.59	-0.33
El Niño Modoki Index	0.50	-0.34

Supplemental Table 3 | Correlation and cumulative residual values for BMM and ARM model scenarios at variable karst residence times (τ). Variable **τ**'s were selected for each model based on significantly correlated R values ≥ 0.85 ($p<0.05$).

BMM Reservoir A: Reservoir B (τ in weeks)	**Pearson's correlation coefficient**	**cumulative residual**
Best case (Figure 2B)	0.93	50.05
40:60 (41 weeks)	0.85	78.01
40:60 (42 weeks)	0.86	77.72
40:60 (43 weeks)	0.86	77.81
40:60 (51 weeks)	0.87	79.95
40:60 (67 weeks)	0.89	83.09
40:60 (80 weeks)	0.87	87.58
40:60 (84 weeks)	0.86	88.86
80:20 (41 weeks)	0.85	102.31
80:20 (42 weeks)	0.86	100.86
80:20 (43 weeks)	0.86	99.73
80:20 (51 weeks)	0.87	92.2
80:20 (67 weeks)	0.89	73.29
80:20 (80 weeks)	0.87	73.2
80:20 (84 weeks)	0.86	75.9
ARM (τ in weeks)	**Pearson's correlation coefficient**	**cumulative residual**
L2 (42 weeks)	0.85	130.07
L2 (67 weeks)	0.89	91.21
L2 (84 weeks)	0.85	85.26
WF (18 weeks)	0.89	126.28
WS (18 weeks)	0.93	123.18

REFERENCES

Aggarwal, P. K., Romatschke, U., Araguas-Araguas, L., Belachew, D., Longstaffe, F. J., Berg, P., Schumacher, C., and Funk, A. (2016). Proportions of convective and stratiform precipitation revealed in water isotope ratios. *Nature Geoscience*, *9*(8), 624.

Akers, P. D., Brook, G. A., Railsback, L. B., Liang, F., Iannone, G., Webster, J. W., Reeder, P.P, Cheng, H., and Edwards, R. L. (2016). An extended and higher-resolution record of climate and land use from stalagmite MC01 from Macal Chasm, Belize, revealing connections between major dry events, overall climate variability, and Maya sociopolitical changes. *Palaeogeography, palaeoclimatology, palaeoecology*, *459*, 268-288.

Bar-Matthews, M., Ayalon, A., Kaufman, A., and Wasserburg, G. J. (1999). The Eastern Mediterranean paleoclimate as a reflection of regional events: Soreq cave, Israel. *Earth and Planetary Science Letters*, *166*(1-2), 85-95.

Baker, A., and Brunsdon, C. (2003). Non-linearities in drip water hydrology: an example from Stump Cross Caverns, Yorkshire. *Journal of Hydrology*, *277*(3-4), 151-163.

Baker, A., Hartmann, A., Duan, W., Hankin, S., Comas-Bru, L., Cuthbert, M. O., Treble, P.C., Banner, J., Genty, D., Baldini, L.M., Bartolomé, M., Moreno, A., Pérez-Mejias, C., and Werner, M. (2019). Global analysis reveals climatic controls on the oxygen isotope composition of cave drip water. *Nature communications*, *10*(1), 2984.

Beal, L. K., Wong, C. I., Bautista, K. K., Jenson, J. W., Banner, J. L., Lander, M. A., Gingerich, S.B., Partin, J.W., Hardt, B., and van Oort, N. H. (2019). Isotopic and geochemical assessment of the sensitivity of groundwater resources of Guam, Mariana Islands, to intra-and inter-annual variations in hydroclimate. *Journal of hydrology*, *568*, 174-183.

Bellenger, H., Guilyardi, É., Leloup, J., Lengaigne, M., & Vialard, J. (2014). ENSO representation in climate models: from CMIP3 to CMIP5. *Climate Dynamics*, *42*(7-8), 1999-2018.

Bowen, G. J., & Wilkinson, B. (2002). Spatial distribution of δ18O in meteoric precipitation. *Geology*, *30*(4), 315-318.

Burns, S. J., Matter, A., Frank, N., & Mangini, A. (1998). Speleothem-based paleoclimate record from northern Oman. *Geology*, *26*(6), 499-502.

Cai, B., Pumijumnong, N., Tan, M., Muangsong, C., Kong, X., Jiang, X., and Nan, S. (2010). Effects of intraseasonal variation of summer monsoon rainfall on stable isotope and growth rate of a stalagmite from northwestern Thailand. *Journal of Geophysical Research: Atmospheres*, *115*(D21).

Cai, W., Borlace, S., Lengaigne, M., Van Rensch, P., Collins, M., Vecchi, G., Timmermann, A., Santoso, A., McPhaden, M.J., Wu, L., England, M. H., Guilyardi, E., and Jin, F.-F. (2014). Increasing frequency of extreme El Niño events due to greenhouse warming. *Nature climate change*, *4*(2), 111.

Cai, Z., and Tian, L. (2016). Processes governing water vapor isotope composition in the Indo-Pacific region: convection and water vapor transport. *Journal of Climate*, *29*(23), 8535-8546.

Carolin, S. A., Cobb, K. M., Adkins, J. F., Clark, B., Conroy, J. L., Lejau, S., Malang, J., and Tuen, A. A. (2013). Varied response of western Pacific hydrology to climate forcings over the last glacial period. *Science*, *340*(6140), 1564-1566.

Carolin, S. A., Cobb, K. M., Lynch-Stieglitz, J., Moerman, J. W., Partin, J. W., Lejau, S., Malang, J., Clark, B., Tuens, A.A., and Adkins, J. F. (2016). Northern Borneo stalagmite records reveal West Pacific hydroclimate across MIS 5 and 6. *Earth and Planetary Science Letters*, *439*, 182-193.

Chadwick, R., Boutle, I., and Marin, G. (2013). Spatial Patterns of Precipitation Change in CMIP5: Why the Rich do not get richer in the tropics, Journal of Climate, 26, 3803 – 3822, doi: 10.1175/JCLI-D-12-00543.1.

Chen, S., Hoffmann, S. S., Lund, D. C., Cobb, K. M., Emile-Geay, J., and Adkins, J. F. (2016). A high-resolution speleothem record of western equatorial Pacific rainfall: Implications for Holocene ENSO evolution. *Earth and Planetary Science Letters*, *442*, 61-71.

Chen, C. J., and Li, T. Y. (2018). Geochemical characteristics of cave drip water respond to ENSO based on a 6-year monitoring work in Yangkou Cave, Southwest China. *Journal of hydrology*, *561*, 896-907.

Cheng, H., Sinha, A., Cruz, F. W., Wang, X., Edwards, R. L., d'Horta, F. M., Ribas, C.C., Vuille, M., Stott, L.D., and Auler, A. S. (2013). Climate change patterns in Amazonia and biodiversity. *Nature communications*, *4*, 1411.

Clark, I. D., & Fritz, P. (2013). *Environmental isotopes in hydrogeology*. CRC press.

Cobb, K. M., Adkins, J. F., Partin, J. W., and Clark, B. (2007). Regional-scale climate influences on temporal variations of rainwater and cave dripwater oxygen isotopes in northern Borneo. *Earth and Planetary Science Letters*, *263*(3-4), 207-220.

Collins, M., An, S. I., Cai, W., Ganachaud, A., Guilyardi, E., Jin, F. F., Jochum, M., Lengaigne, M., Power, S., Timmermann, A., Vecchi, G., and Wittenberg, A. (2010). The impact of global warming on the tropical Pacific Ocean and El Niño. *Nature Geoscience*, *3*(6), 391.

Comas-Bru, L., and Harrison, S. P. (2019). SISAL: Bringing added value to speleothem research.

Conroy, J. L., Cobb, K. M., and Noone, D. (2013). Comparison of precipitation isotope variability across the tropical Pacific in observations and SWING2 model simulations. *Journal of Geophysical Research: Atmospheres*, *118*(11), 5867-5892.

Craig, H. (1961). Isotopic variations in meteoric waters. *Science*, *133*(3465), 1702-1703.
Crawford, J., Hughes, C. E., & Lykoudis, S. (2014). Alternative least squares methods for determining the meteoric water line, demonstrated using GNIP data. *Journal of Hydrology*, *519*, 2331-2340.

Cruz Jr, F. W., Burns, S. J., Karmann, I., Sharp, W. D., Vuille, M., Cardoso, A. O., Ferrari, J.A., Silva Dias, P.L., and Viana Jr, O. (2005). Insolation-driven changes in atmospheric circulation over the past 116,000 years in subtropical Brazil. *Nature*, *434*(7029), 63.

Cuthbert, M. O., Baker, A., Jex, C. N., Graham, P. W., Treble, P. C., Andersen, M. S., and Acworth, R. I. (2014). Drip water isotopes in semi-arid karst: implications for speleothem paleoclimatology. *Earth and Planetary Science Letters*, *395*, 194-204.

Dansgaard, W. (1964). Stable isotopes in precipitation. *Tellus*, *16*(4), 436-468.

Dansgaard, W., Johnsen, S. J., Clausen, H. B., Dahl-Jensen, D., Gundestrup, N. S., Hammer, C. U., Hvldberg, C.S., Steffensen, J.P., Sveinbjörnsdottir, A.E., Jouzel, J., and Bond, G. (1993). Evidence for general instability of past climate from a 250-kyr ice-core record. *Nature*, *364*(6434), 218.

Dee, S., Emile-Geay, J., Evans, M. N., Allam, A., Steig, E. J., & Thompson, D. M. (2015). PRYSM: An open-source framework for PRoxY System Modeling, with applications to oxygen-isotope systems. *Journal of Advances in Modeling Earth Systems*, *7*(3), 1220-1247.

Dettman, D.L., and Lohmann, K.C., 1995. Microsampling carbonates for stable isotope and minor element analysis: physical separation of samples on a 20 micrometer scale. Journal of Sedimentary Research A65, 566 – 569.

Edwards, R. L., Chen, J. H., and Wasserburg, G. J. (1987). 238U234U230Th232Th systematics and the precise measurement of time over the past 500,000 years. *Earth and Planetary Science Letters*, *81*(2-3), 175-192.

Evans, M. N., Tolwinski-Ward, S. E., Thompson, D. M., and Anchukaitis, K. J. (2013). Applications of proxy system modeling in high resolution paleoclimatology. *Quaternary science reviews*, *76*, 16-28.

Fairchild, I. J., Smith, C. L., Baker, A., Fuller, L., Spötl, C., Mattey, D., and McDermott, F. (2006). Modification and preservation of environmental signals in speleothems. *Earth-Science Reviews*, *75*(1-4), 105-153.

Fairchild, I. J., & Baker, A. (2012). Speleothem science: from process to past environments (Vol. 3). John Wiley & Sons.

Faure, G., & Mensing, T. M. (2005). Isotopes: principles and applications. John Wiley & Sons.

Fleitmann, D., Burns, S. J., Mudelsee, M., Neff, U., Kramers, J., Mangini, A., & Matter, A. (2003). Holocene forcing of the Indian monsoon recorded in a stalagmite from southern Oman. *science*, *300*(5626), 1737-1739.

Fleitmann, D., Burns, S. J., Neff, U., Mudelsee, M., Mangini, A., and Matter, A. (2004). Palaeoclimatic interpretation of high-resolution oxygen isotope profiles derived from annually laminated speleothems from Southern Oman. *Quaternary Science Reviews*, *23*(7-8), 935-945.

Ford, D., and Williams, P. D. (2013). *Karst hydrogeology and geomorphology*. John Wiley & Sons.

Frappier, A. B., Sahagian, D., Carpenter, S. J., González, L. A., and Frappier, B. R. (2007). Stalagmite stable isotope record of recent tropical cyclone events. *Geology*, *35*(2), 111-114.

Frappier, A., Sahagian, D., Gonzalez, L.A., and Carpenter, S.J., 2002. El Niño events recorded by stalagmite carbon isotopes. Science 298, 565.

Gascoyne, M. (1992). Palaeoclimate determination from cave calcite deposits. *Quaternary Science Reviews*, *11*(6), 609-632.

Genty, D., & Quinif, Y. (1996). Annually laminated sequences in the internal structure of some Belgian stalagmites; importance for paleoclimatology. *Journal of Sedimentary Research*, *66*(1), 275-288.

Gillieson, D., and Clark, B. (2010). Mulu: The World's Most Spectacular Tropical Karst, in Geomorphological Landscapes of the World, edited, pp. 311 – 320, Springer.

Glynn, P. W., & De Weerdt, W. H. (1991). Elimination of Two Reef-Building Hydrocorals Following the 1982-83 El Niño Warming Event. *Science*, *253*(5015), 69-71.

Griffiths, M. L., Drysdale, R. N., Gagan, M. K., Zhao, J. X., Ayliffe, L. K., Hellstrom, J. C., Hantoro, W.S., Frisia, S., Feng, Y.-x, Cartwright, I., Pierre, E. S., Fischer, M.J., and Suwargadi, B.W. (2009). Increasing Australian–Indonesian monsoon rainfall linked to early Holocene sea-level rise. *Nature Geoscience*, *2*(9), 636.

Heinrich, H. (1988). Origin and consequences of cyclic ice rafting in the northeast Atlantic Ocean during the past 130,000 years. *Quaternary research*, *29*(2), 142-152.

Hoefs, J. (2004). Stable Isotope Geochemistry, 5th ed., Springer, New York, NY.

Jex, C. N., Baker, A., Fairchild, I. J., Eastwood, W. J., Leng, M. J., Sloane, H. J., Thomas, L., and Bekaroğlu, E. (2010). Calibration of speleothem δ18O with instrumental climate records from Turkey. *Global and Planetary Change*, *71*(3-4), 207-217.

Jones, I. C., and Banner, J. L. (2003). Estimating recharge thresholds in tropical karst island aquifers: Barbados, Puerto Rico and Guam. *Journal of Hydrology*, *278*(1-4), 131-143.

Jones, I. C., Banner, J. L., and Humphrey, J. D. (2000). Estimating recharge in a tropical karst aquifer. *Water Resources Research*, *36*(5), 1289-1299.

Kendall, C., & McDonnell, J. J. (Eds.). (2012). *Isotope tracers in catchment hydrology*. Elsevier.

Kennett, D. J., Breitenbach, S. F., Aquino, V. V., Asmerom, Y., Awe, J., Baldini, J. U., Bartlein, P., Culleton, B.J., Ebert, C., Jazwa, C., Macri, M. J., Marwan, N., Polyak, V., Prufer, K.M., Ridley, H.E., Sodemann, H., Winterhalder, B., and Huag, G.H. (2012). Development and disintegration of Maya political systems in response to climate change. *Science*, *338*(6108), 788-791.

Konecky, B. L., Noone, D. C., and Cobb, K. M. (2019). The Influence of Competing Hydroclimate Processes on Stable Isotope Ratios in Tropical Rainfall. *Geophysical Research Letters*, *46*(3), 1622-1633.

Kurita, N. (2013). Water isotopic variability in response to mesoscale convective system over the tropical ocean. *Journal of Geophysical Research: Atmospheres*, *118*(18), 10-376.
Lachniet, M. S., Bernal, J. P., Asmerom, Y., Polyak, V., and Piperno, D. (2012). A 2400 yr Mesoamerican rainfall reconstruction links climate and cultural change. *Geology*, *40*(3), 259-262.

Lachniet, M. S., Burns, S. J., Piperno, D. R., Asmerom, Y., Polyak, V. J., Moy, C. M., and Christenson, K. (2004). A 1500-year El Niño/Southern Oscillation and rainfall history for the isthmus of Panama from speleothem calcite. *Journal of Geophysical Research: Atmospheres*, *109*(D20).

Lases-Hernandez, F., Medina-Elizalde, M., Burns, S., and DeCesare, M. (2019). Long-term monitoring of drip water and groundwater stable isotopic variability in the Yucatán Peninsula: Implications for recharge and speleothem rainfall reconstruction. *Geochimica et Cosmochimica Acta*, *246*, 41-59.

Liu, S., Peng, X., Chen, Q., Qin, S., Zhao, J., Feng, Y., Luo, S., and Zhou, H. (2018). The 1997–1998 El Niño event recorded by a stalagmite from central China. *Quaternary international*, *487*, 71-77.

Lu, Z., Liu, Z., Zhu, J., & Cobb, K. (2018). A review of paleo El Niño-southern oscillation. *Atmosphere*, *9*(4), 130.

Majoube, M. (1971). Oxygen-18 and deuterium fractionation between water and steam. J. Chim. Phys-Chim. Biol. 69(10).

Maupin, C.R., Partin, J.W., Shen, C.-C., Quinn, T.M., Lin, K., Taylor, F.W., Banner, J.L, Thirumalai, K., Sinclair, D.J. (2014). Persistent decadal-scale rainfall variability in the tropical South Pacific Convergence Zone through the past six centuries. *Clim. Past,* 10(4), 1319 – 1332.

McDonald, J., Drysdale, R., Hill, D., Chisari, R., and Wong, H. (2007). The hydrochemical response of cave drip waters to sub-annual and inter-annual climate variability, Wombeyan Caves, SE Australia. *Chemical Geology*, *244*(3-4), 605-623.

Meckler, A. N., Clarkson, M. O., Cobb, K. M., Sodemann, H., and Adkins, J. F. (2012). Interglacial hydroclimate in the tropical West Pacific through the Late Pleistocene. *Science*, *336*(6086), 1301-1304.

Medina-Elizalde, M., Burns, S. J., Lea, D. W., Asmerom, Y., von Gunten, L., Polyak, V., Vuille, M., and Karmalkar, A. (2010). High resolution stalagmite climate record from the Yucatán Peninsula spanning the Maya terminal classic period. *Earth and Planetary Science Letters*, *298*(1-2), 255-262.

Mickler, P. J., Banner, J. L., Stern, L., Asmerom, Y., Edwards, R. L., and Ito, E. (2004). Stable isotope variations in modern tropical speleothems: evaluating equilibrium vs. kinetic isotope effects. *Geochimica et Cosmochimica Acta*, *68*(21), 4381-4393.

Moerman, J. W., Cobb, K. M., Adkins, J. F., Sodemann, H., Clark, B., and Tuen, A. A. (2013). Diurnal to interannual rainfall δ18O variations in northern Borneo driven by regional hydrology. *Earth and Planetary Science Letters*, *369*, 108-119.

Moerman, J. W., Cobb, K. M., Partin, J. W., Meckler, A. N., Carolin, S. A., Adkins, J. F., Lejau, S., Malang, J., Clark, B., and Tuen, A. A. (2014). Transformation of ENSO-related rainwater to dripwater δ18O variability by vadose water mixing. *Geophysical Research Letters*, *41*(22), 7907-7915.

Mook, W., and Rozanski, K. (2000). Environmental isotopes in the hydrological cycle. *IAEA Publish*, *39*.

Moquet, J. S., Cruz, F. W., Novello, V. F., Stríkis, N. M., Deininger, M., Karmann, I., Ventura Santos, R., Millo, C., Apaestegui, J., Guyot, J.-L., Siffedine, A., Vuille, M., Cheng,

H., Edwards, R.L., and Santini, W. (2016). Calibration of speleothem δ18O records against hydroclimate instrumental records in Central Brazil. *Global and Planetary Change*, *139*, 151-164.

Muangsong, C., Cai, B., Pumijumnong, N., Hu, C., and Cheng, H. (2014). An annually laminated stalagmite record of the changes in Thailand monsoon rainfall over the past 387 years and its relationship to IOD and ENSO. *Quaternary international*, *349*, 90-97.

Nakagawa, M., Tanaka, K., Nakashizuka, T., Ohkubo, T., Kato, T., Maeda, T., Sato, K., Miguchi, H., Nagamasu, H., Ogino, K., Teo, S., Hamid, A.A., and Seng, L.H. (2000). Impact of severe drought associated with the 1997–1998 El Nino in a tropical forest in Sarawak. *Journal of Tropical Ecology*, *16*(3), 355-367.

Nott, J., Haig, J., Neil, H., and Gillieson, D. (2007). Greater frequency variability of landfalling tropical cyclones at centennial compared to seasonal and decadal scales. *Earth and Planetary Science Letters*, *255*(3-4), 367-372.

Novello, V. F., Cruz, F. W., Vuille, M., Stríkis, N. M., Edwards, R. L., Cheng, H., Emerick, S., de Paula, M.S., Li, X., Barreto, E.S., Karmann, I., and Santos, R.V. (2017). A high-resolution history of the South American Monsoon from Last Glacial Maximum to the Holocene. *Scientific reports*, *7*, 44267.

Okazaki, A., Satoh, Y., Tremoy, G., Vimeux, F., Scheepmaker, R., and Yoshimura, K. (2015). Interannual variability of isotopic composition in water vapor over western Africa and its relationship to ENSO. *Atmospheric Chemistry and Physics*, *15*(6), 3193-3204.

Orland, I.J., Burstyn, Y., Bar-Matthews, M., Kozdon, R., Ayalon, A., Matthews, A., Valley, J.W. (2014). Seasonal climate signals (1990 – 2008) in a modern Soreq Cave stalagmite as revealed by high-resolution geochemical Analysis. *Chem. Geol.* 363, 203 – 215.

PAGES Hydro2k Consortium. (2017). Comparing proxy and model estimates of hydroclimate variability and change over the Common Era. *Climate of the Past*, *13*(12), 1851-1900.

Partin, J. W., Cobb, K. M., Adkins, J. F., Clark, B., and Fernandez, D. P. (2007). Millennial-scale trends in west Pacific warm pool hydrology since the Last Glacial Maximum. *Nature*, *449*(7161), 452.

Partin, J. W., Jenson, J. W., Banner, J. L., Quinn, T. M., Taylor, F. W., Sinclair, D., Hardt, B., Lander M.A., Bell, T., Miklavic, B., Jocson, J. M., and Taborosi, D. (2012). Relationship between modern rainfall variability, cave dripwater, and stalagmite geochemistry in Guam, USA. *Geochemistry, Geophysics, Geosystems*, *13*(3).

Partin, J. W., Cobb, K. M., Adkins, J. F., Tuen, A. A., and Clark, B. (2013a). Trace metal and carbon isotopic variations in cave dripwater and stalagmite geochemistry from northern Borneo. *Geochemistry, Geophysics, Geosystems*, *14*(9), 3567-3585.

Partin, J. W., Quinn, T. M., Shen, C. C., Emile-Geay, J., Taylor, F. W., Maupin, C. R., Lin, K., Jackson, C.S., Banner, J.L., Sinclair, D.J., Huh, C. A. (2013b). Multidecadal rainfall variability in South Pacific Convergence Zone as revealed by stalagmite geochemistry. *Geology*, *41*(11), 1143-1146.

Rozanski, K., Araguas-Araguas, L., and Gonfiantini, R. (1992). Relation between long-term trends of oxygen-18 isotope composition of precipitation and climate. *Science*, *258*(5084), 981-985.

Rozanski, K., Araguás-Araguás, L., & Gonfiantini, R. (1993). Isotopic patterns in modern global precipitation. *Climate change in continental isotopic records*, *78*, 1-36.

Sánchez-Murillo, R., Birkel, C., Welsh, K., Esquivel-Hernández, G., Corrales-Salazar, J., Boll, J., Brooks, E., Roupsard, O., Sáenz-Rosales, O., Katchan, I., Arce-Mesén, R., Soulsby, C., Araguás-Araguás, L.J. (2016). Key drivers controlling stable isotope variations in daily precipitation of Costa Rica: Caribbean Sea versus Eastern Pacific Ocean moisture sources. *Quaternary Science Reviews*, *131*, 250-261.

Sinha, A., Cannariato, K. G., Stott, L. D., Li, H. C., You, C. F., Cheng, H., Edwards, R.L., Singh, I. B. (2005). Variability of Southwest Indian summer monsoon precipitation during the Bølling-Allerød. *Geology*, *33*(10), 813-816.

Spötl, C., and Mangini, A. (2002). Stalagmite from the Austrian Alps reveals Dansgaard–Oeschger events during isotope stage 3:: Implications for the absolute chronology of Greenland ice cores. *Earth and Planetary Science Letters*, *203*(1), 507-518.

State of the Tropics (2017). State of the Tropics 2017 Report. University JC, Townsville, Australia.

Sun, Z., Yang, Y., Zhao, J., Tian, N., and Feng, X. (2018). Potential ENSO effects on the oxygen isotope composition of modern speleothems: Observations from Jiguan Cave, central China. *Journal of hydrology*, *566*, 164-174.

Sweeting, M.M. (1980). The Geomorphology of Mulu: An Introduction, The Geographical Journal, 146(1), 1 – 7.

Tan, M. (2014). Circulation effect: response of precipitation δ18O to the ENSO cycle in monsoon regions of China. *Climate Dynamics*, *42*(3-4), 1067-1077.

Treble, P. C., Bradley, C., Wood, A., Baker, A., Jex, C. N., Fairchild, I. J., Gagan, M.K., Cowley, J., and Azcurra, C. (2013). An isotopic and modelling study of flow paths and

storage in Quaternary calcarenite, SW Australia: implications for speleothem paleoclimate records. *Quaternary Science Reviews*, *64*, 90-103.

Treble, P., Shelley, J. M. G., and Chappell, J. (2003). Comparison of high resolution sub-annual records of trace elements in a modern (1911–1992) speleothem with instrumental climate data from southwest Australia. *Earth and Planetary Science Letters*, *216*(1-2), 141-153.

Wang, G., Cai, W., Gan, B., Wu, L., Santoso, A., Lin, X., Chen, Z., and McPhaden, M. J. (2017). Continued increase of extreme El Niño frequency long after 1.5 C warming stabilization. *Nature Climate Change*, *7*(8), 568.

Wang, X., Auler, A. S., Edwards, R. L., Cheng, H., Ito, E., and Solheid, M. (2006). Interhemispheric anti-phasing of rainfall during the last glacial period. *Quaternary Science Reviews*, *25*(23-24), 3391-3403.

Wang, Y. J., Cheng, H., Edwards, R. L., An, Z. S., Wu, J. Y., Shen, C. C., and Dorale, J. A. (2001). A high-resolution absolute-dated late Pleistocene monsoon record from Hulu Cave, China. *science*, *294*(5550), 2345-2348.

Waltham, A.C., and Brook, D.B. (1980). Cave development in the Melinau Limestone of the Gunung Mulu National Park, The Geographical Journal, 146(2), 258 – 266.

Weedon, G.P., 2003. Time-Series Analysis and Cyclostratigraphy. CUP, Cambridge.

Wong, C. I., and Breecker, D. O. (2015). Advancements in the use of speleothems as climate archives. *Quaternary Science Reviews*, *127*, 1-18.

Zhang, H., Cheng, H., Spötl, C., Cai, Y., Sinha, A., Tan, L., Yi, L., Yan, H., Kathayat, G., Ning Y., Li, X., Zhang, F., Zhao, J., and Edwards, R.L. (2018). A 200-year annually laminated stalagmite record of precipitation seasonality in southeastern China and its linkages to ENSO and PDO. *Scientific reports*, *8*(1), 12344.

Zhang, J., and Li, T.Y. (2019). Seasonal and interannual variations of hydrochemical characteristics and stable isotopic compositions of drip waters in Furong Cave, Southwest China based on 12 years' monitoring. Journal of Hydrology. 572. 10.1016/j.jhydrol.2019.02.052.

Zwart, C., Munksgaard, N. C., Protat, A., Kurita, N., Lambrinidis, D., & Bird, M. I. (2018). The isotopic signature of monsoon conditions, cloud modes, and rainfall type. *Hydrological processes*, *32*(15), 2296-2303.